

**Citation** M. Prabhushankar and G AlRegib, "Introspective Learning : A Two-Stage Approach for Inference in Neural Networks" *Advances in Neural Information Processing Systems* (2022), Nov 29 - Dec 1, 2022.

**Review** Data of Submission : 19 May 2022  
Date of Revision : 2 Aug 2022  
Date of Accept: 14 Sept 2022

**Codes** <https://github.com/olivesgatech/Introspective-Learning>

**Copyright** The authors grant NeurIPS a non-exclusive, perpetual, royalty-free, fully-paid, fully-assignable license to copy, distribute and publicly display all or parts of the paper. Personal use of this material is permitted. Permission from the authors must be obtained for all other uses, in any current or future media, including reprinting/republishing this material for advertising or promotional purposes, for resale or redistribution to servers or lists.

**Contact** mohit.p@gatech.edu OR alregib@gatech.edu  
<https://ghassanalregib.info/>

---

# Introspective Learning : A Two-Stage Approach for Inference in Neural Networks

---

**Mohit Prabhushankar**  
Electrical and Computer Engineering  
Georgia Institute of Technology  
Atlanta, GA 30308  
mohit.p@gatech.edu

**Ghassan AlRegib**  
Electrical and Computer Engineering  
Georgia Institute of Technology  
Atlanta, GA 30308  
alregib@gatech.edu

## Abstract

In this paper, we advocate for two stages in a neural network’s decision making process. The first is the existing feed-forward inference framework where patterns in given data are sensed and associated with previously learned patterns. The second stage is a slower reflection stage where we ask the network to reflect on its feed-forward decision by considering and evaluating all available choices. Together, we term the two stages as introspective learning. We use gradients of trained neural networks as a measurement of this reflection. A simple three-layered Multi Layer Perceptron is used as the second stage that predicts based on all extracted gradient features. We perceptually visualize the *post-hoc* explanations from both stages to provide a visual grounding to introspection. For the application of recognition, we show that an introspective network is 4% more robust and 42% less prone to calibration errors when generalizing to noisy data. We also illustrate the value of introspective networks in downstream tasks that require generalizability and calibration including active learning, out-of-distribution detection, and uncertainty estimation. Finally, we ground the proposed machine introspection to human introspection for the application of image quality assessment.

## 1 Introduction

Introspection is the act of looking into one’s own mind [1]. Classical introspection has its roots in philosophy. Locke [2], the founder of empiricism, held that all human ideas come from experience. This experience is a result of both sensation and reflection. By sensation, one receives passive information using the sensory systems of sight, sound, and touch. Reflection is the objective observation of our own mental operations. Consider the toy example in Fig. 1. Given an image  $x$  and an objective of recognizing  $x$ , we first sense some key features in the bird. These features include the color and shape of the body, feathers and beak. The features are chosen based on our existing notion of what is required to contrast between birds. We then associate these features with our existing knowledge of birds and make a coarse decision that  $x$  is a spoonbill. This is the sensing stage. Reflection involves questioning the coarse decision and asking why  $x$  cannot be a Flamingo, Crane, Pig or any other class. If the answers are satisfactory, then an introspective decision that  $x$  is indeed a spoonbill is made. The observation of this reflection is introspection.

In this paper, we adopt this differentiation between sensing and reflection to advocate for two-stage neural network architectures for perception-based applications. Specifically, we consider classification. The sensing stage is any existing feed-forward neural network including VGG [3], ResNet [4], and DenseNet [5] architectures among others. These networks sense patterns in  $x$  and make a coarse feed-forward decision,  $\hat{y}$ . The second stage examines this decision by reflecting on the introspective question ‘Why  $\hat{y}$ , rather than  $y_I$ ?’ where  $y_I$  is any introspective class that the sensing network has learned. Note that there is no external intervention or new information that informs

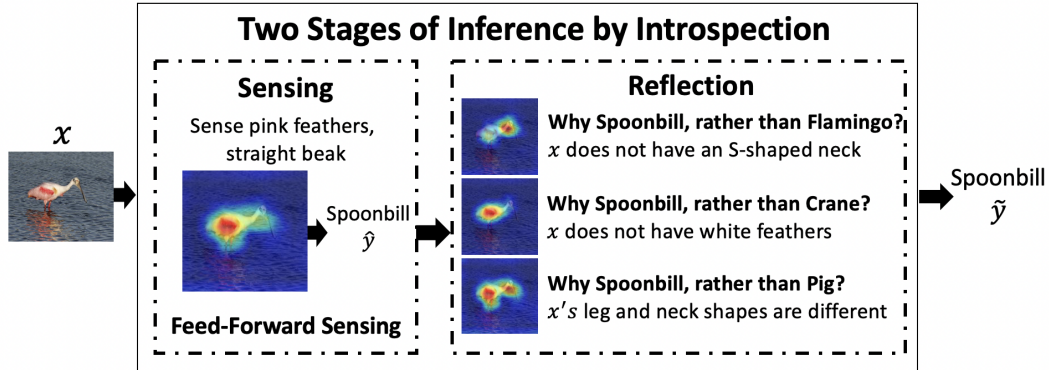


Figure 1: Example of the introspection process. The visual *post-hoc* explanations are from Grad-CAM [6] framework using the proposed features. Additional heatmaps along with the generation process is provided in Appendix A. The written text is for illustrative purpose only.

the reflection stage. Hence, the introspective features are *post-hoc* in the sense that they are not causal answers to the introspective questions but rather, are the network’s notion of the answers. This is inline with the original definition of introspection which is that introspection is the observation of existing knowledge reflected upon by the network. These *post-hoc* introspective features are visualized using Grad-CAM [6] in the reflection stage of Fig. 1.

The challenge that we address in this paper is in defining the reflection stage in terms of neural networks. The authors in [7], utilize the same intuition to construct a *reflective stage* composed of explanations. However, when the train and test distributions are dissimilar, the predictions and hence the explanations are incorrect. We overcome this by considering alternative questions for the explanation. Consider any dataset with  $N$  classes. A network trained on this dataset will have  $N$  possible introspective questions and answers, similar to the ones shown in Fig. 1. Our goal is to implicitly extract features that answer all  $N$  introspective questions without explicitly training on said features. This involves 1) implicitly creating introspective questions, 2) answering the posed questions to obtain introspective features, and 3) predicting the output  $\tilde{y}$  from the introspective features. We show that gradients w.r.t network parameters store notions about the difference between classes and can be used as introspective features. We use an MLP termed  $\mathcal{H}(\cdot)$ , as our introspective network that combines all features to predict  $\tilde{y}$ . A limitation of the proposed method is the size of  $N$  which is discussed in Sections 3.

We show that the introspective prediction  $\tilde{y}$  is robust to noise. An intuition for this robustness is that not only should the network sense the feed-forward patterns, it must also satisfy  $\mathcal{H}(\cdot)$ ’s  $N$  notions of difference between classes. Hence, during inference, we extract  $N$  additional features that inform the introspective prediction  $\tilde{y}$ . The main contributions of this paper are the following:

1. We define implicit introspective questions that allow for reflection in a neural network. This reflection is measured using loss gradients w.r.t. network parameters across all possible introspective classes in Section 3.
2. We provide a methodology to efficiently extract introspective loss gradients and combine them using a second  $\mathcal{H}(\cdot)$  MLP network in Section 4.
3. We illustrate  $\mathcal{H}(\cdot)$ ’s robust and calibrated nature in Section 6. We validate the effectiveness of this generalization in downstream applications like active learning, out-of-distribution detection, uncertainty estimation, and Image Quality Assessment in Appendix D.

## 2 Background

### 2.1 Introspective questions, features, and network

**Introspective questions** The choice of ‘*Why  $\hat{y}$ , rather than  $y_1$ ?*’ is not arbitrary. The authors in [8] describe three questions that complete *post-hoc* explanations - correlation, counterfactual, and contrastive questions. These questions together allow for an alternate form of reasoning within neural networks called abductive reasoning. The sensing network predicts based on correlations.

Since, we do not intervene within the data during the reflection stage, counterfactual questions cannot be answered. Hence, we use contrastive questions as our introspective questions. Further details regarding abductive reasoning and our choice of question is provided in Appendix A.

**Gradients as Introspective Features** The gradients from a base network have been utilized in diverse applications including *post-hoc* visual explanations [6, 9, 10], adversarial attacks [11], uncertainty estimation [12], anomaly detection [13, 14], and saliency detection [15] among others. Fisher Vectors use gradients of generative models to characterize the change that data creates within features [16]. [17] uses gradients of parameters to characterize the change in manifolds when new data is introduced to an already trained manifold. Our framework uses the intuition from [17] to characterize changes for a datapoint that is perceived as new, due to it being assigned an introspective class  $y_I$ , that is different from its predicted class  $\hat{y}$ . In [18], the authors view the network as a graph and intervene within it to obtain *holographic* features. Our introspective features are also *holographic* in the sense that they characterize the change between  $\hat{y}$  and  $y_I$  without changing the network. However, our features do not require interventions that become expensive with scale.

**Two-stage networks** The usage of two-stage approaches to inference in neural networks is not new. In [7], the authors extract Grad-CAM explanations from feed-forward networks to train a *reflective stage*. However, our framework involves reflecting on all contrastive questions rather than correlation questions. The authors in [19] propose SimCLR, a self-supervised framework where multiple data augmentation strategies are used to contrastively train an overhead MLP. The MLP provides features which are stored as a dictionary. This feature dictionary is used as a look-up table for new test data. In this paper, we use gradients against all classes as features and an MLP  $\mathcal{H}(\cdot)$ , to predict on these features. [20] and [21] consider all classes in a conditional maximum likelihood estimate on test data to retrain the model. These works differ from ours in our usage of the base sensing network. [22] uses gradients and activations together as features and note that the validity of gradients as features is in pretrained base networks rather than additional parameters from the two-stage networks. This adds to our argument of using two-stage networks but with loss gradients against introspective classes.

## 2.2 Feed-forward Features

For the application of recognition, a sensing neural network  $f(\cdot)$  is trained on a distribution  $\mathcal{X}$  to classify data into  $N$  classes. The network learns notions about data samples when classifying them. These notions are stored as network weights  $W$ . Given a data sample  $x$ ,  $f(x)$  is a projection on the network weights. Let  $y_{feat}$  be the logits projected before the final fully connected layer. In the final fully connected layer  $f_L(\cdot)$ , the parameters  $W_L$  can be considered as  $N$  filters each of dimensionality  $d_{L-1} \times 1$ . The output of the network  $\hat{y}$  is given by,

$$\begin{aligned} y_{feat} &= f_{L-1}(x), \forall y \in \mathbb{R}^{N \times 1}, \\ \hat{y} &= \arg \max(W_L^T y_{feat}), \forall W_L \in \mathbb{R}^{d_{L-1} \times N}, f_{L-1}(x) \in \mathbb{R}^{d_{L-1} \times 1}. \end{aligned} \quad (1)$$

Here  $\hat{y}$  is the feed-forward inference and  $y_{feat}$  are the feed-forward features. In this paper, we compare our introspective features against feed-forward features. Since introspection occurs after  $f(\cdot)$ , all our results are *plug-in* on top of existing  $f(\cdot)$ .

## 3 Introspective Features

In this section, we describe introspective features and implicitly extract them using the sensing network. We then analyze them for sparsity, efficiency, and robustness.

**Definition 3.1** (Introspection). *Given a network  $f(\cdot)$ , a datum  $x$ , and the network’s prediction  $f(x) = \hat{y}$ , introspection in  $f(\cdot)$  is the measurement of change induced in the network parameters when a label  $y_I$  is introduced as the label for  $x$ . This measurement is the gradient induced by a loss function  $J(y_I, \hat{y})$ , w.r.t. the network parameters.*

This definition for introspection is in accordance with the sensing and reflection stages in Fig. 1. The network’s prediction  $\hat{y}$  is the output of the sensing stage and the change induced by an introspective label,  $y_I$ , is the network reflecting on its decision  $\hat{y}$  as opposed to  $y_I$ . Note that introspection can occur when  $\hat{y}$  is contrasted against any trained label  $y_I, I \in [1, N]$ . For instance, in Fig. 1, the network is asked to reflect on its decision of spoonbill by considering other  $y_I$  that  $x$  can take - flamingo, crane, or pig. These results are extracted from ImageNet [23] and hence,  $I \in [1, 1000]$ . Additional visual introspective saliency maps similar to Fig. 1 are provided in Appendix A.

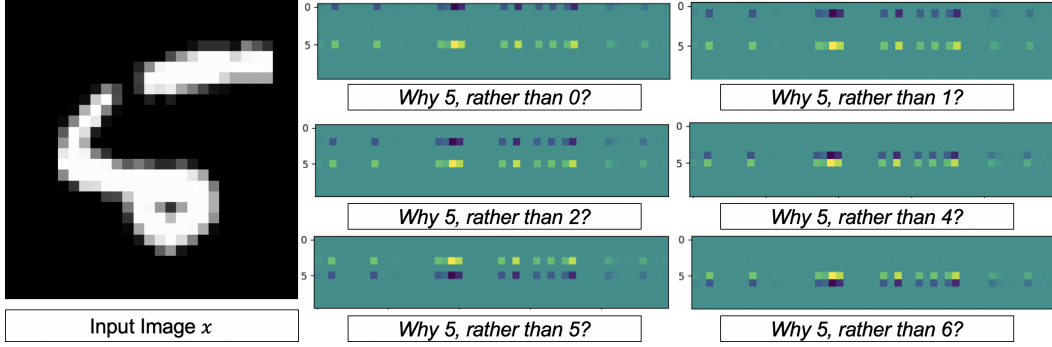


Figure 2: For the input image on the left, the  $\nabla_{W_L} J(y_I, 5)$  are shown on the right. Each image is a visualization of the  $50 \times 10$  gradient matrix. All images are sparse except in the prediction row 5 and introspective question row  $i$ .

Reflection is the empirical risk that the network has predicted  $x$  as  $\hat{y}$  instead of  $y_I$ . Given the network parameters, this risk is measured through some loss function  $J(y_I, \hat{y})$ .  $y_I$  is a one-hot vector with a one at the  $I^{th}$  location. The change that is induced in the network is given by the gradient of  $J(y_I, \hat{y})$  w.r.t. the network parameters. For an  $N$ -class classifier, there are  $N$  possible introspective classes and hence  $N$  possible gradients each given by,  $r_I = \nabla_W J(y_I, \hat{y}), I \in [1, N]$ . Here,  $r_I$  are the introspective features. Since we introspect based on classes, we measure the change in network weights in the final fully connected layer. Therefore, the introspective features are given by,

$$r_I = \nabla_{W_L} J(y_I, \hat{y}), I \in [1, N], r_I \in \mathbb{R}^{d_{L-1} \times N} \quad (2)$$

where  $W_L$  are the network weights for the final fully connected layer. Note that the final fully connected layer from Eq. 1 has a dimensionality of  $\mathbb{R}^{d_{L-1} \times N}$ . For every  $x$ , Eq. 2 is applied  $N$  times to obtain  $N$  separate  $r_I$ . We first analyze these features.

### 3.1 Sparsity and Robustness of Introspective Features

Consider  $r_I$  in Eq. 2. Each  $r_I$  is a  $d_{L-1} \times N$  matrix. Expressing gradients in  $r_I$  separately w.r.t. the different filters in  $W_L$ , we have a row-wise concatenated set of gradients given by,

$$r_I = [\nabla_{W_{L,1}} J(y_I, \hat{y}); \nabla_{W_{L,2}} J(y_I, \hat{y}); \nabla_{W_{L,3}} J(y_I, \hat{y}) \dots \nabla_{W_{L,N}} J(y_I, \hat{y})] \quad (3)$$

where each  $W_{L,j} \in \mathbb{R}^{d_{L-1} \times 1}$  and  $r_I \in \mathbb{R}^{d_{L-1} \times N^2}$ . For all data  $x \in \mathcal{X}$  the following lemma holds:

**Lemma 1.** *Given a unique ordered pair  $(x, \hat{y})$  and a well-trained network  $f(\cdot)$ , the gradients for a loss function  $J(y_I, \hat{y})$  w.r.t. classes are pairwise orthogonal under the second-order Taylor series approximation, each class paired with the predicted class.*

*Proof.* Provided in Appendix B.1. □

**Sparsity** Lemma 1 states that backpropagating class  $y_I$  does not provide any information to  $W_{L,j}, j \neq I$  and hence there is no need to use  $\nabla_{W_{L,j}} J(y_j, \hat{y}), j \neq i$  as features when considering  $y_I$ . The proof is provided in Appendix B.1.  $\nabla_W J(y_I, \hat{y})$  for an introspective class reduces to,

$$\nabla_W J(y_I, \hat{y}) = -\nabla_W y_I + \nabla_W \log \left( 1 + \frac{y_{\hat{y}}}{2} \right). \quad (4)$$

where  $y_{\hat{y}}$  is the logit associated with the predicted class. We demonstrate the sparsity of Eq. 4 in Fig. 2. A two-layer CNN is trained on MNIST [24] dataset with a test accuracy exceeding 99%. This satisfies the condition for Lemma 1 that  $f(\cdot)$  is well-trained. The final fully connected layer in this network has a size of  $50 \times 10$ . We provide an input image  $x$  of number 5 to a trained network as shown in Fig. 2. The network correctly identifies the image as a 5. We then backpropagate the introspective class 0 using  $J(5, 0)$  with  $\hat{y} = 5$  and  $y_I = 0$ . This answers the question ‘Why 5, rather

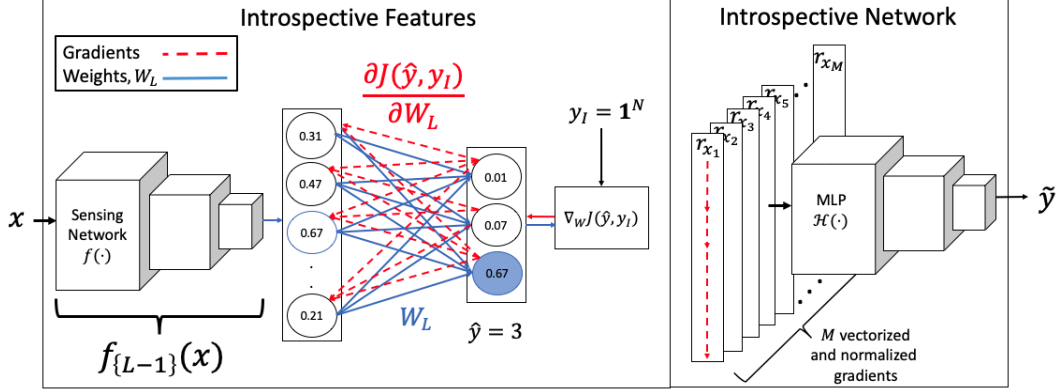


Figure 3: Introspective Learning process. Once  $r_x$  for all images in the dataset are generated, an introspective network  $\mathcal{H}(\cdot)$  is trained. During testing, the noisy image is passed through sensing network  $f(\cdot)$ , extraction module to generate  $r_x$  and finally through the introspective network  $\mathcal{H}(\cdot)$ .

than 0?'. The gradient features in the final fully connected layer are the same dimensions as the final fully connected layer,  $50 \times 10$  or more generally  $\mathcal{O}(d_{L-1} \times N)$ . This matrix is displayed as a normalized image in Fig. 2. Yellow scales to 1 and blue is  $-1$  while green is 0. It can be seen that the only values present in the matrix are negative at  $W_{L,0}$ , in blue, and positive in  $W_{L,5}$ , in yellow. This validates Eq. 5 that for a fully-trained network the only values, and hence the only information, required from  $W_L$  for  $I = 0$  is  $\nabla_{W_{L,0}}$ . We show the matrix  $\nabla_{W_L}$  when  $I = 0, 1, 2, 4, 5, 6$ . The difference among all matrices is the location of the negative values that exist at  $\nabla_{W_{L,I}}$  for different values of  $I$ .

**Robustness** Eq. 4 motivates the generalizable nature of introspective features. Consider some noise added to  $x$ . To change the prediction  $\hat{y}$ , the noise must sufficiently decrease  $y_{\hat{y}}$  from Eq. 4 and increase the closest logit value,  $y_I$ , to change the prediction. Hence, it needs to change one orthogonal relationship. However, by constraining our final prediction  $\tilde{y}$  on  $N$  such features, the noise needs to change the orthogonal relationship between  $N$  pairwise logits. This motivates an introspective network  $\mathcal{H}(\cdot)$  that is conditioned on all  $N$  pairwise logits.

### 3.2 Efficient Extraction of Introspective Features

From Lemma 1, the introspective feature is only dependent on the predicted class  $\hat{y}$  and the introspective class  $y_I$  making their span orthogonal to all other gradients. Hence,

$$r_I = \nabla_{W_{L,I}} J(y_I, \hat{y}), I \in [1, N], r_I \in \mathbb{R}^{d_{L-1} \times 1} \quad (5)$$

Building on Lemma 1, we present the following theorem.

**Theorem 1.** *Given a unique ordered pair  $(x, \hat{y})$  and a well-trained network  $f(\cdot)$ , the gradients for a loss function  $J(y_I, \hat{y}), I \in [1, N]$  w.r.t. classes when  $y_I$  are  $N$  orthogonal one-hot vectors is equivalent to when  $y_I$  is a vector of all ones, under the second-order Taylor series approximation.*

*Proof.* Provided in Appendix B.2. □

The proof follows Lemma 1. Theorem 1 states that backpropagating a vector of all ones ( $\mathbf{1}_N$ ) is equivalent to backpropagating  $N$  one-hot vectors with ones at orthogonal positions. This reduces the time complexity from  $\mathcal{O}(N)$  to a constant  $\mathcal{O}(1)$  since we only require a single pass to backpropagate  $\mathbf{1}_N$ . Hence, our introspective feature is given by,

$$r_x = \nabla_{W_L} J(\mathbf{1}_N, \hat{y}), r_x \in \mathbb{R}^{d_{L-1} \times N}, \mathbf{1}_N = \mathbf{1}^{N \times 1} \quad (6)$$

Note the LHS is now  $r_x$  instead of  $r_I$  from Eq. 5. The final introspective feature is a matrix of the same size as  $W_L$  extracted in  $\mathcal{O}(1)$  time with a space complexity of  $\mathcal{O}(d_{L-1} \times N)$ .  $r_x$  is vectorized and scaled between  $[-1, 1]$  before being used in Sections 4 and 6 as introspective features. This procedure is illustrated in Fig. 3

## 4 Introspective Network

Once  $r_x$  are extracted using Eq. 6, the introspective label  $\hat{y}$  from Fig. 3 is given by  $\hat{y} = \mathcal{H}(r_x)$  where  $\mathcal{H}(\cdot)$  is an MLP. In this section, we analyze  $\mathcal{H}(\cdot)$ . From Fig. 3,  $f(\cdot)$  is any existing trained network used to obtain introspective features  $r_x$ . It is trained to predict the ground truth  $y$  given any  $x$ . Based on the assumption that  $\mathcal{H}(r_x) = \mathbb{E}(y|f(x))$  and hence expectation of  $y - \mathcal{H}(r_x)$  is 0, the loss function can be decomposed as,

$$\mathbb{E}[(f(x) - y)^2] = \mathbb{E}[(f(x) - \mathcal{H}(r_x))^2] + \mathbb{E}[(\mathcal{H}(r_x) - y)^2]. \quad (7)$$

Note that since the goal is to predict  $y$  given  $x$ ,  $\mathcal{H}(r_x) = \mathbb{E}(y|f(x))$  is a fair assumption to make. Substituting for  $f(x)$  in Eq. 7, and using variance decomposition of  $y$  onto  $f(x)$ , we have,

$$\mathbb{E}[(\hat{y} - y)^2] = \text{Var}(\hat{y}) - \text{Var}(\mathcal{H}(r_x)) + \mathbb{E}[(\mathcal{H}(r_x) - y)^2]. \quad (8)$$

This decomposition is adopted from structured calibration techniques. A full derivation is presented in [25]. The first term  $\text{Var}(\hat{y})$  is the the variance in the prediction from  $f(\cdot)$ . This term is the precision of  $f(\cdot)$  and is low for a well trained network. The third term is the MSE function between the introspective network  $\mathcal{H}(\cdot)$  and the ground truth. It is minimized while training the  $\mathcal{H}(\cdot)$  network. The second term is the variance of the network  $\mathcal{H}(\cdot)$ , given features  $r_x$ . Note that minimizing Eq. 8 can occur by maximizing  $\text{Var}(\mathcal{H}(r_x))$ . We use a fisher vector interpretation from [17] to analyze  $\text{Var}(\mathcal{H}(r_x))$ . If  $\mathcal{H}(\cdot)$  is a linear layer with parameters  $W_{\mathcal{H}}$ , the  $\text{Var}(\mathcal{H}(r_x))$  term reduces to  $W_{\mathcal{H}}^T W_{\mathcal{H}} \times \text{Var}(r_x) \propto \text{Tr}(r_x^T \Sigma^{-1} r_x)$  where  $\Sigma$  is the covariance matrix.  $\Sigma$  is a gaussian approximation for the shape of the manifold. Generalizing it to a higher dimensional manifold and replacing  $\Sigma$  with  $F$ , we have,

$$\text{Var}(\mathcal{H}(r_x)) = \text{Tr}(r_x^T F^{-1} r_x), \quad (9)$$

$$\text{Var}(\mathcal{H}(r_x)) = \sum_{j=1}^N r_j^T F^{-1} r_j. \quad (10)$$

The RHS of Eq. 10 is a sum of fisher vectors taken across all possible labels.

**When do introspective networks provide robustness?** We use Eq. 10 to analyze introspective learning usage. Specifically, we consider two cases: When input  $x$  is taken from the training distribution  $\mathcal{X}$ , and when it is taken from a noisy distribution  $\mathcal{X}'$ .

1. When a sample  $x \in \mathcal{X}$  is provided to a network  $f(\cdot)$  trained on  $\mathcal{X}$ , all  $r_j, j \neq \hat{y}$  in Eq. 10 tend to 0. The RHS reduces to  $r_{\hat{y}}^T F^{-1} r_{\hat{y}}$ .  $r_{\hat{y}}$  is a function of  $f(x)$  only and hence adds no new information to the framework. The results of  $\mathcal{H}(\cdot)$  remain the same as  $f(\cdot)$ . In other words, given a trained ResNet-18 on CIFAR-10, the results of feed-forward learning will be the same as introspective learning on CIFAR-10 testset.
2. When a new sample  $x' \notin \mathcal{X}$  is provided to a network  $f(\cdot)$  trained on  $\mathcal{X}$ , a fisher vector based projection across labels is more descriptive compared to a feed-forward approach. The  $N$  gradients in Eq. 10 add new information based on how the network needs to change the manifold shape  $F$  to accommodate the introspective gradients. Hence, given a distorted version of CIFAR-10 testset, our proposed introspective learning generalizes with a higher accuracy while providing calibrated outputs from Eq. 8. We empirically illustrate these claims in Section 6. We motivate other applications including active learning, Out-Of-Distribution (OOD) detection, uncertainty estimation, and Image Quality Assessment (IQA) that are dependent on generalizability and calibration in Section 5.

## 5 Related Works for Considered Applications

**Augmentations and Robustness** The considered  $r_x$  features from Eq. 6 can be considered as feature augmentations. Augmentations, including SimCLR [19], Augmix [26], adversarial augmentation [27], and noise augmentations [28] have shown to increase robustness of neural networks. We use introspection on top of non-augmented and augmented (Section 6) networks and show that our proposed two-stage framework increases the robustness to create generalizable and calibrated inferences which aids active learning and out-of-distribution (OOD) detection. The same framework that robustly recognizes images despite noise can also detect noise to make an out-of-distribution detection.

**Confidence and Uncertainty** The existence of adversarial images [11] heuristically decouples the probability of neural network predictions from confidence and uncertainty. A number of works including [29] and [30] use bayesian formulation to provide uncertainty. However, in downstream tasks like active learning and Out-Of-Distribution (OOD) detection applications, existing state-of-the-art methods utilize softmax probability as confidences. This is because of the simplicity and ease of numerical computation of softmax. In active learning, uncertainty is quantified by the entropy [31], least confidence [31], or maximum margin [32] of predicted logits, or through extracted features in BADGE [33], and BALD [34]. In OOD detection, [35] proposes Maximum Softmax Probability (MSP) as a baseline method by creating a threshold function on the softmax output. [36] proposes ODIN and improves on MSP by calibrating the network’s softmax probability using temperature scaling [37]. In this paper, we show that the proposed introspective features are better calibrated than their feed-forward counterparts. Hence existing methods in active learning and OOD detection have a superior performance when using  $\mathcal{H}(\cdot)$  to make predictions.

**Human Introspection** We are unaware of any direct application that tests visual human introspection. In its absence, we choose the application of Full-Reference Image Quality Assessment (FR-IQA) to connect machine vision with human vision. The goal in FR-IQA is to objectively estimate the subjective quality of an image. Humans are shown a pristine image along with a distorted image and asked to score the quality of the distorted image [38]. This requires reflection on the part of the observers. We take an existing algorithm [39] and show that introspecting on top of this IQA technique brings its assessed scores closer to human scores.

## 6 Experiments

Across all applications except in Ablation studies in Table 9, we use a 3-layered MLP with sigmoid activations as  $\mathcal{H}(\cdot)$ . The structure is presented in Appendix C.1. We first define robustness and calibration in the context of this paper.

**Robustness** In this paper, without loss of consistency with related works, we say that the network trained on distribution  $\mathcal{X}$  is robust if it correctly predicts on a shifted distribution  $\mathcal{X}'$ . The difference in data distributions can be because of data acquisition setups, environmental conditions, distortions among others. We use CIFAR-10 for  $\mathcal{X}$  and two distortion datasets - CIFAR-10C [27] and CIFAR-10-CURE [40] as  $\mathcal{X}'$ . Generalization is measured through performance accuracy.

**Calibration** Given a data distribution  $x \in \mathcal{X}$ , belonging to any of  $y \in [1, N]$ , a neural network provides two outputs - the decision  $\hat{y}$  and the confidence associated with  $\hat{y}$ , given by  $\hat{p}$ . Let  $p$  be the true probability empirically estimated as  $p = \hat{p}_i, \forall i \in [1, M]$ . Then calibration is given by [37],

$$\mathbb{P}(y = \hat{y} | p = \hat{p}) = p \tag{11}$$

Calibration measures the difference between the confidence levels and the prediction accuracy. To showcase calibration we use the metric of Expected Calibration Error (ECE) as described in [37]. The network predictions are placed in 10 separate bins based on their prediction confidences. Ideally, the accuracy equals the mid-point of confidence bins. The difference between accuracy and mid-point of bins, across bins is measured by ECE. Lower the ECE, better calibrated is the network.

**Datasets and networks** CIFAR-10C consists of 950,000 images whose purpose is to evaluate the robustness of networks trained on original CIFAR-10 trainset. CIFAR-10C perturbs the CIFAR-10 testset using 19 distortions in 5 progressive levels. Hence, there are 95 separate  $\mathcal{X}'$  distributions to test on with each  $\mathcal{X}'$  consisting of 10000 images. Note that we are not using any distortions or data from CIFAR-10C as a validation split during training. The authors in [40] provide realistic distortions that they used to benchmark real-world recognition applications including Amazon Rekognition and Microsoft Azure. We use these distortions to perturb the test set of CIFAR-10. There are 6 distortions, each with 5 progressive levels. Of these 6 distortions - Salt and Pepper, Over Exposure, and Under Exposure noises are new compared to CIFAR-10C. We train four ResNet architectures - ResNet-18, 34, 50, and 101 [4]. All four ResNets are evaluated as sensing networks  $f(\cdot)$ . The training procedure and hyperparameters are presented in Appendix C.1.

**Testing on CIFAR-10 testset** The trained networks are tested on CIFAR-10 testset with accuracies 91.02%, 93.01%, 93.09%, and 93.11% respectively. Next we extract  $r_x$  on all training and testing images in CIFAR-10.  $\mathcal{H}(\cdot)$  is trained using  $r_x$  from the trainset using the same procedure as  $f(\cdot)$ . When tested on  $r_x$  of the testset, the accuracy for ResNets-18,34,50,101 is 90.93%, 92.92%, 93.17%,



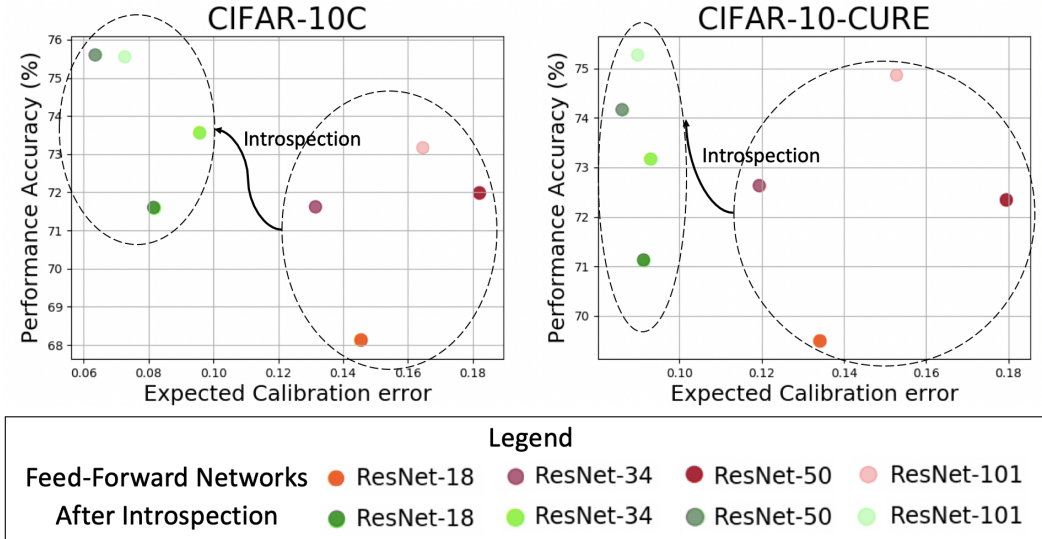


Figure 4: Scatter plot with performance accuracy vs expected calibration error. Ideally, networks are in top left. Introspectivity increases performance accuracy while decreasing calibration error.

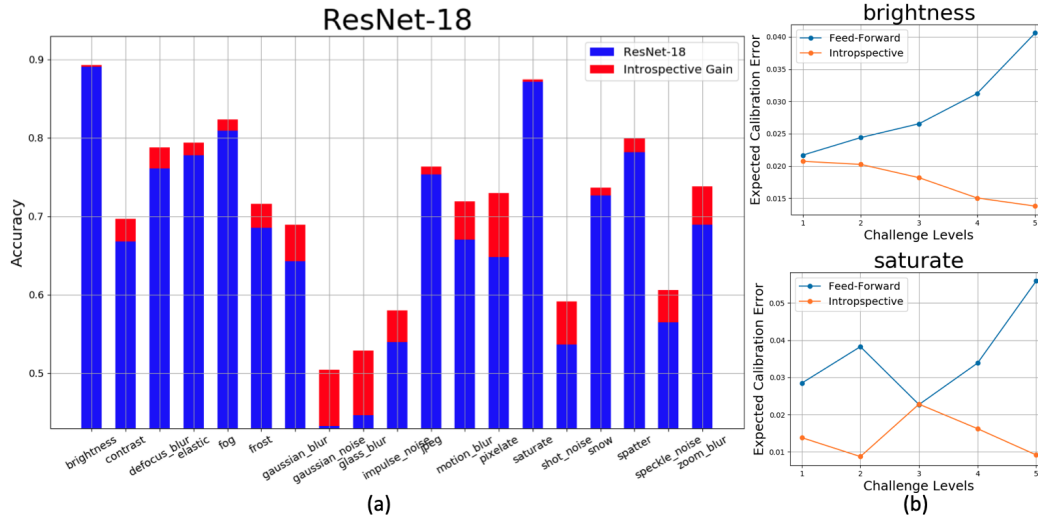


Figure 5: (a) ResNet-18 on CIFAR-10C. (b) Expected calibration error across 5 challenge levels in brightness and saturate distortions. Note that both these distortions do not affect the performance of the network and their feed-forward accuracy is high. The improvement in accuracy is statistically insignificant. However, introspection decreases the ECE across challenge levels.

and 93.03%. Note that this is similar to the feed-forward results. The average ECE of all feed-forward and introspective networks is 0.04. Hence, when the test distribution is the same as training distribution there is no change in performance.

**Testing on CIFAR-10C and CIFAR-10-CURE** The results of all networks averaged across distortions in both the datasets are shown in Fig. 4. Note that in each case, there is a shift leftward and upward indicating that the performance improves while the calibration error decreases. In the larger CIFAR-10C dataset, the introspective ResNet-18 performs similar to ResNets-34 and 50 in terms of accuracy while beating them both in calibration. A more fine-grained analysis is shown in Fig. 5 for ResNet-18. The blue bars in Fig. 5a) represent the feed-forward accuracy. The red bars are the introspective accuracy gains over the feed-forward accuracy. Among 7 of the 19 distortions, the accuracy gains are over 5%. In Appendix C.2.1, we see that the gains are higher when the distortions are higher. Introspection performs well on blur-like distortions while struggling with distortions that disrupt the lower level characteristics of the image like brightness, contrast, and saturate. This can be attributed to the fact that  $r_x$  are derived from the last layer of  $f(\cdot)$  and are missing low-level

statistics that are filtered out by network in the initial layers. However, in Fig. 5b), we show ECE for brightness and saturate distortions across all 5 distortion levels - higher the level, more is the distortion affecting  $\mathcal{X}'$ . It can be seen that while the ECE for feed-forward networks increases across levels, the ECE for introspective networks decrease. Hence, even when there are no accuracy gains to be had, introspection helps in calibration.

**Plug-in results of Introspection** Note that there are a number of techniques proposed to alleviate a neural network’s robustness challenges against distortions.

Table 1: Introspecting on top of existing robustness techniques.

METHODS		ACCURACY
RESNET-18	FEED-FORWARD	67.89%
	INTROSPECTIVE	<b>71.4%</b>
DENOISING	FEED-FORWARD	65.02%
	INTROSPECTIVE	<b>68.86%</b>
ADVERSARIAL TRAIN [27]	FEED-FORWARD	68.02%
	INTROSPECTIVE	<b>70.86%</b>
SIMCLR [19]	FEED-FORWARD	70.28%
	INTROSPECTIVE	<b>73.32%</b>
AUGMENT NOISE [28]	FEED-FORWARD	76.86%
	INTROSPECTIVE	<b>77.98%</b>
AUGMIX [26]	FEED-FORWARD	89.85%
	INTROSPECTIVE	<b>89.89%</b>

The authors in [28] show that finetuning VGG-16 using blurry training images increases the performance of classification under blurry conditions. [41] propose utilizing distorted virtual images to boost performance accuracy. The authors in [27] use adversarial images to augment the training data. All these works require knowledge of distortion or large amounts of new data during training. Our proposed method can infer introspectively on top of any existing  $f(\cdot)$  enhanced using existing methods. In Table 1, we show results of introspection as a *plug-in* approach on top of existing techniques. In all methods, introspection outperforms its feed-forward counterpart. While introspecting on top of Augmix, trained on WideResNet [26] provides insignificant recognition accuracy gains, introspection reduces ECE of Augmix network by 43.33%. In Appendix C.2, we show performance on top of [28] and [27] of 6.8% on Level 5 distortions. In Appendix C.3, we analyze SimCLR and show that introspecting on the self supervised features increases its CIFAR-10C performance by about 6% on ResNet-101. A number of ablation studies including analysis of structure of  $\mathcal{H}(\cdot)$ , loss functions, distortion levels on performance accuracy and ECE are shown in Appendix C.4. Moreover, we examine introspection when  $\mathcal{X}'$  is domain shifted data from Office [42] dataset in Appendix C.6.1.

**Downstream Applications** We consider four downstream applications: Active Learning, Out-of-Distribution detection, Uncertainty estimation, and Image Quality Assessment (IQA) to demonstrate the validity of introspection. Similar to recognition experiments, in all considered applications there is a distributional difference between train and testset. We show results that conform to Eq. 10. We show statistically significant introspective IQA results in Appendix D.3 and Table 13, and uncertainty estimation results in Appendix D.4.

**Active Learning** The goal in active learning is to decrease the test error in a model by choosing the *best* samples from a large pool of unlabeled data to annotate and train the model. A number of strategies are proposed to query the *best* samples. A full review of active learning and query strategies are given in [43]. Existing active learning strategies define *best* samples to annotate as those samples that the model is either most uncertain about. This uncertainty is quantified by either entropy [31], least confidence [31], maximum margin [32], or through extracted features in BADGE [33], and BALD [34]. We show the results of ResNet-18 and 34 architecture in Table 2. Implementations of all query strategies in Table 2 are taken from the codebase of [33] and reported as Feed-Forward results. Note that the query strategies act on  $f(\cdot)$  to sample images at every round. Instead of sampling on  $f(\cdot)$ , all query strategies sample using  $\mathcal{H}(\cdot)$  in the Introspective results. The training, testing, and all strategies are the same as Feed-Forward from [33]. Doing so we find similar results as recognition - on the original testset the active learning results are the same while there is a gain across strategies on Gaussian noise testset from CIFAR-10C. Note that the results shown are averaged over 20 rounds with a query batch size of a 1000 and initial random choice - which were kept same for  $f(\cdot)$  and  $\mathcal{H}(\cdot)$  - of 100. Further details, plots, and variances are shown in Appendix D.1.

**Out-of-distribution Detection** The goal of Out-Of-Distribution (OOD) detection is to detect those samples that are drawn from a distribution  $\mathcal{X}' \neq \mathcal{X}$  given a fully trained  $f(\cdot)$ . A number of techniques are proposed to detect out-of-distribution samples. The authors in [35] propose Maximum Softmax Probability (MSP) as a baseline method by creating a threshold function on the softmax output. The authors in [36] propose ODIN and improved on MSP by calibrating the network’s softmax probability using temperature scaling [37]. In this paper, we illustrate that applying existing methods when applied on  $\mathcal{H}(\cdot)$ , their detection performance is greater than if they were applied on the feed-forward

Table 2: Recognition accuracy of Active Learning strategies.

Methods	Architecture	Original Testset		Gaussian Noise	
		R-18	R-34	R-18	R-34
Entropy [31]	Feed-Forward	0.365	0.358	0.244	0.249
	Introspective	0.365	0.359	<b>0.258</b>	<b>0.255</b>
Least [31]	Feed-Forward	0.371	0.359	0.252	0.25
	Introspective	0.373	0.362	<b>0.264</b>	<b>0.26</b>
Margin [32]	Feed-Forward	0.38	0.369	0.251	0.253
	Introspective	0.381	0.373	<b>0.265</b>	<b>0.263</b>
BALD [34]	Feed-Forward	0.393	0.368	0.26	0.253
	Introspective	0.396	0.375	<b>0.273</b>	<b>0.263</b>
BADGE [33]	Feed-Forward	0.388	0.37	0.25	0.247
	Introspective	0.39	0.37	<b>0.265</b>	<b>0.260</b>

Table 3: Out-of-distribution Detection of existing techniques compared between feed-forward and introspective networks.

Methods	OOD Datasets	FPR (95% at TPR)	Detection Error	AUROC
		↓	↓	↑
Feed-Forward/Introspective				
MSP [35]	Textures	58.74/ <b>19.66</b>	18.04/ <b>7.49</b>	88.56/ <b>97.79</b>
	SVHN	61.41/ <b>51.27</b>	16.92/ <b>15.67</b>	89.39/ <b>91.2</b>
	Places365	58.04/ <b>54.43</b>	17.01/ <b>15.07</b>	89.39/ <b>91.3</b>
	LSUN-C	<b>27.95</b> /27.5	<b>9.42</b> /10.29	<b>96.07</b> /95.73
ODIN [36]	Textures	52.3/ <b>9.31</b>	22.17/ <b>6.12</b>	84.91/ <b>91.9</b>
	SVHN	66.81/ <b>48.52</b>	23.51/ <b>15.86</b>	83.52/ <b>91.07</b>
	Places365	<b>42.21</b> /51.87	16.23/ <b>15.71</b>	<b>91.06</b> /90.95
	LSUN-C	<b>6.59</b> /23.66	<b>5.54</b> /10.2	<b>98.74</b> /95.87

$f(\cdot)$ . The code for OOD detection techniques are taken from [44] along with all hyperparameters and the training regimen for their reported DenseNet [5] architecture. The temperature scaling coefficient for ODIN is set to 1000. Note that we do not use temperature scaling on  $\mathcal{H}$ , to illustrate the effectiveness of our method. We use three established metrics to evaluate OOD detection - False Positive Rate (FPR) at 95% True Positive Rate (TPR), Detection error, and AUROC. Ideally, AUROC values for a given method is high while the other two metrics are low. We use CIFAR-10 as our in-distribution dataset and use four OOD datasets - SVHN [45], Describable Textures Dataset [46], Places 365 [47], and LSUN [48]. The results are presented in Table 3. Note that among the four datasets, textures and SVHN are *more* out-of-distribution from CIFAR-10 than the natural image datasets of Places365 and LSUN. The results of the introspective network is highest on Textures DTD dataset and gets progressively worse among the natural image datasets. Further analysis on networks and methods, along with their training regimen is provided in Appendix D.2.

## 7 Discussion and Conclusion

**Limitations and future work** The paper illustrates the benefits of utilizing the change in model parameters as a measure of model introspection. In Section 3.2, we accelerate the time complexity to  $\mathcal{O}(1)$ . However, the space complexity is still dependent on  $N$ . The paper uses an MLP for  $\mathcal{H}(\cdot)$  and constructs  $r_x$  by vectorizing extracted gradients. For datasets with large  $N$ , usage of  $r_x$  as a vector is prohibitive. Hence, a required future work is to provide a method of combining all  $N$  gradients without vectorization. Also, our implementation uses serial gradient extraction across images. This is non-ideal since the available GPU resources are not fully utilized. A parallel implementation with per-sample gradient extraction [49] is a pertinent acceleration technique for the future.

**Broader and Societal Impact** In his seminal book in 2011 [50], Daniel Kahneman outlines two systems of thought and reasoning in humans - a fast and instinctive ‘system 1’ that heuristically associates sensed patterns followed by a more deliberate and slower ‘system 2’ that examines and analyzes the data in context of intrinsic biases. Our framework derives its intuition based on these two systems of reasoning. The introspective explanations can serve to examine the intrinsic notions and biases that a network uses to categorize data. Note that the network  $\mathcal{H}(\cdot)$  obtains its introspective answers through  $f(\cdot)$ . Hence, similar to the ‘system 2’ reasoning in humans, any internal bias present in  $f(\cdot)$  only gets strengthened in  $\mathcal{H}(\cdot)$  through confirmation bias. The framework will benefit from a human intervention between  $f(\cdot)$  and  $\mathcal{H}(\cdot)$  in sensitive applications. One way would be to ask counterfactual questions by providing an established counterfactual and asking the network to reflect based on that. While the introspective framework will remain the same, the features will change.

**Conclusion** We introduce the concept of introspection in neural networks as two separate stages in a network’s decision process - the first is making a quick assessment based on sensed patterns in data and the second is reflecting on that assessment based on all possible decisions that could have been taken and making a final decision based on this reflection. We show that doing so increases the generalization performance of neural networks as measured against distributionally shifted data while reducing the calibration error of neural networks. Existing state-of-the-art methods in downstream tasks like active learning and out-of-distribution detection perform better in an introspective setting compared to a feed-forward setting especially when the distributional difference is high.

## References

- [1] Edwin G Boring, “A history of introspection.,” *Psychological bulletin*, vol. 50, no. 3, pp. 169, 1953.
- [2] John Locke, *An essay concerning human understanding*, Kay & Troutman, 1847.
- [3] Karen Simonyan and Andrew Zisserman, “Very deep convolutional networks for large-scale image recognition,” in *International Conference on Learning Representations*, 2015.
- [4] Kaiming He, Xiangyu Zhang, Shaoqing Ren, and Jian Sun, “Deep residual learning for image recognition,” in *Proceedings of the IEEE conference on computer vision and pattern recognition*, 2016, pp. 770–778.
- [5] Gao Huang, Zhuang Liu, Laurens Van Der Maaten, and Kilian Q Weinberger, “Densely connected convolutional networks,” in *Proceedings of the IEEE conference on computer vision and pattern recognition*, 2017, pp. 4700–4708.
- [6] Ramprasaath R Selvaraju, Michael Cogswell, Abhishek Das, Ramakrishna Vedantam, Devi Parikh, and Dhruv Batra, “Grad-cam: Visual explanations from deep networks via gradient-based localization,” in *Proceedings of the IEEE international conference on computer vision*, 2017, pp. 618–626.
- [7] Johannes Schneider and Michalis Vlachos, “Reflective-net: Learning from explanations,” *arXiv preprint arXiv:2011.13986*, 2020.
- [8] Ghassan AlRegib and Mohit Prabhushankar, “Explanatory paradigms in neural networks: Towards relevant and contextual explanations,” *IEEE Signal Processing Magazine*, vol. 39, no. 4, pp. 59–72, 2022.
- [9] Mohit Prabhushankar, Gukyeong Kwon, Dogancan Temel, and Ghassan AlRegib, “Contrastive explanations in neural networks,” in *2020 IEEE International Conference on Image Processing (ICIP)*. IEEE, 2020, pp. 3289–3293.
- [10] Mohit Prabhushankar and Ghassan AlRegib, “Extracting causal visual features for limited label classification,” in *2021 IEEE International Conference on Image Processing (ICIP)*. IEEE, 2021, pp. 3697–3701.
- [11] Ian J Goodfellow, Jonathon Shlens, and Christian Szegedy, “Explaining and harnessing adversarial examples,” *arXiv preprint arXiv:1412.6572*, 2014.
- [12] Jinsol Lee and Ghassan AlRegib, “Gradients as a measure of uncertainty in neural networks,” in *2020 IEEE International Conference on Image Processing (ICIP)*. IEEE, 2020, pp. 2416–2420.
- [13] Gukyeong Kwon, Mohit Prabhushankar, Dogancan Temel, and Ghassan AlRegib, “Backpropagated gradient representations for anomaly detection,” in *European Conference on Computer Vision*. Springer, 2020, pp. 206–226.
- [14] Gukyeong Kwon, Mohit Prabhushankar, Dogancan Temel, and Ghassan AlRegib, “Novelty detection through model-based characterization of neural networks,” in *2020 IEEE International Conference on Image Processing (ICIP)*. IEEE, 2020, pp. 3179–3183.
- [15] Yutong Sun, Mohit Prabhushankar, and Ghassan AlRegib, “Implicit saliency in deep neural networks,” in *2020 IEEE International Conference on Image Processing (ICIP)*. IEEE, 2020, pp. 2915–2919.
- [16] Tommi S Jaakkola, David Haussler, et al., “Exploiting generative models in discriminative classifiers,” *Advances in neural information processing systems*, pp. 487–493, 1999.
- [17] David A Cohn, “Neural network exploration using optimal experiment design,” 1994.
- [18] Martin A Zinkevich, Alex Davies, and Dale Schuurmans, “Holographic feature representations of deep networks.,” in *UAI*, 2017.
- [19] Ting Chen, Simon Kornblith, Mohammad Norouzi, and Geoffrey Hinton, “A simple framework for contrastive learning of visual representations,” in *International conference on machine learning*. PMLR, 2020, pp. 1597–1607.
- [20] Aurick Zhou and Sergey Levine, “Amortized conditional normalized maximum likelihood: Reliable out of distribution uncertainty estimation,” in *International Conference on Machine Learning*. PMLR, 2021, pp. 12803–12812.

- [21] Koby Bibas, Yaniv Fogel, and Meir Feder, “Deep pnml: Predictive normalized maximum likelihood for deep neural networks,” *arXiv preprint arXiv:1904.12286*, 2019.
- [22] Fangzhou Mu, Yingyu Liang, and Yin Li, “Gradients as features for deep representation learning,” *arXiv preprint arXiv:2004.05529*, 2020.
- [23] Jia Deng, Wei Dong, Richard Socher, Li-Jia Li, Kai Li, and Li Fei-Fei, “Imagenet: A large-scale hierarchical image database,” in *2009 IEEE conference on computer vision and pattern recognition*. Ieee, 2009, pp. 248–255.
- [24] Yann LeCun, Léon Bottou, Yoshua Bengio, Patrick Haffner, et al., “Gradient-based learning applied to document recognition,” *Proceedings of the IEEE*, vol. 86, no. 11, pp. 2278–2324, 1998.
- [25] Volodymyr Kuleshov and Percy S Liang, “Calibrated structured prediction,” *Advances in Neural Information Processing Systems*, vol. 28, pp. 3474–3482, 2015.
- [26] Dan Hendrycks, Norman Mu, Ekin D Cubuk, Barret Zoph, Justin Gilmer, and Balaji Lakshminarayanan, “Augmix: A simple data processing method to improve robustness and uncertainty,” *arXiv preprint arXiv:1912.02781*, 2019.
- [27] Dan Hendrycks and Thomas Dietterich, “Benchmarking neural network robustness to common corruptions and perturbations,” *arXiv preprint arXiv:1903.12261*, 2019.
- [28] Igor Vasiljevic, Ayan Chakrabarti, and Gregory Shakhnarovich, “Examining the impact of blur on recognition by convolutional networks,” *arXiv preprint arXiv:1611.05760*, 2016.
- [29] Murat Sensoy, Lance Kaplan, and Melih Kandemir, “Evidential deep learning to quantify classification uncertainty,” *arXiv preprint arXiv:1806.01768*, 2018.
- [30] David JC MacKay, “Probable networks and plausible predictions—a review of practical bayesian methods for supervised neural networks,” *Network: computation in neural systems*, vol. 6, no. 3, pp. 469, 1995.
- [31] Dan Wang and Yi Shang, “A new active labeling method for deep learning,” in *2014 International joint conference on neural networks (IJCNN)*. IEEE, 2014, pp. 112–119.
- [32] Dan Roth and Kevin Small, “Margin-based active learning for structured output spaces,” in *European Conference on Machine Learning*. Springer, 2006, pp. 413–424.
- [33] Jordan T Ash, Chicheng Zhang, Akshay Krishnamurthy, John Langford, and Alekh Agarwal, “Deep batch active learning by diverse, uncertain gradient lower bounds,” *arXiv preprint arXiv:1906.03671*, 2019.
- [34] Yarin Gal, Riashat Islam, and Zoubin Ghahramani, “Deep bayesian active learning with image data,” in *International Conference on Machine Learning*. PMLR, 2017, pp. 1183–1192.
- [35] Dan Hendrycks and Kevin Gimpel, “A baseline for detecting misclassified and out-of-distribution examples in neural networks,” *arXiv preprint arXiv:1610.02136*, 2016.
- [36] Shiyu Liang, Yixuan Li, and Rayadurgam Srikant, “Enhancing the reliability of out-of-distribution image detection in neural networks,” *arXiv preprint arXiv:1706.02690*, 2017.
- [37] Chuan Guo, Geoff Pleiss, Yu Sun, and Kilian Q Weinberger, “On calibration of modern neural networks,” in *International Conference on Machine Learning*. PMLR, 2017, pp. 1321–1330.
- [38] Hamid R Sheikh, Muhammad F Sabir, and Alan C Bovik, “A statistical evaluation of recent full reference image quality assessment algorithms,” *IEEE Transactions on image processing*, vol. 15, no. 11, pp. 3440–3451, 2006.
- [39] Dogancan Temel, Mohit Prabhushankar, and Ghassan AlRegib, “Unique: Unsupervised image quality estimation,” *IEEE signal processing letters*, vol. 23, no. 10, pp. 1414–1418, 2016.
- [40] Dogancan Temel, Jinsol Lee, and Ghassan AlRegib, “Cure-or: Challenging unreal and real environments for object recognition,” in *2018 17th IEEE International Conference on Machine Learning and Applications (ICMLA)*. IEEE, 2018, pp. 137–144.
- [41] Dogancan Temel, Gukyeong Kwon, Mohit Prabhuhankar, and Ghassan AlRegib, “CURE-TSR: Challenging unreal and real environments for traffic sign recognition,” *Advances in Neural Information Processing Systems (NIPS) Machine Learning for Intelligent Transportations Systems Workshop*, 2017.

- [42] Kate Saenko, Brian Kulis, Mario Fritz, and Trevor Darrell, “Adapting visual category models to new domains,” in *European conference on computer vision*. Springer, 2010, pp. 213–226.
- [43] Burr Settles, “Active learning literature survey,” 2009.
- [44] Jiefeng Chen, Yixuan Li, Xi Wu, Yingyu Liang, and Somesh Jha, “Robust out-of-distribution detection for neural networks,” *arXiv preprint arXiv:2003.09711*, 2020.
- [45] Yuval Netzer, Tao Wang, Adam Coates, Alessandro Bissacco, Bo Wu, and Andrew Y Ng, “Reading digits in natural images with unsupervised feature learning,” 2011.
- [46] M. Cimpoi, S. Maji, I. Kokkinos, S. Mohamed, , and A. Vedaldi, “Describing textures in the wild,” in *Proceedings of the IEEE Conf. on Computer Vision and Pattern Recognition (CVPR)*, 2014.
- [47] Bolei Zhou, Agata Lapedriza, Aditya Khosla, Aude Oliva, and Antonio Torralba, “Places: A 10 million image database for scene recognition,” *IEEE transactions on pattern analysis and machine intelligence*, vol. 40, no. 6, pp. 1452–1464, 2017.
- [48] Fisher Yu, Ari Seff, Yinda Zhang, Shuran Song, Thomas Funkhouser, and Jianxiong Xiao, “Lsun: Construction of a large-scale image dataset using deep learning with humans in the loop,” *arXiv preprint arXiv:1506.03365*, 2015.
- [49] Ian Goodfellow, “Efficient per-example gradient computations,” *arXiv preprint arXiv:1510.01799*, 2015.
- [50] Daniel Kahneman, *Thinking, fast and slow*, Macmillan, 2011.
- [51] Wilhelm Max Wundt, *Grundzüge der physiologischen Psychologie*, vol. 1, W. Engelman, 1874.
- [52] Eric Schwitzgebel, “Introspection,” in *The Stanford Encyclopedia of Philosophy*, Edward N. Zalta, Ed. Metaphysics Research Lab, Stanford University, winter 2019 edition, 2019.
- [53] Charles Sanders Peirce, *Collected papers of charles sanders peirce*, Harvard University Press, 1931.
- [54] Gabriele Paul, “Approaches to abductive reasoning: an overview,” *Artificial intelligence review*, vol. 7, no. 2, pp. 109–152, 1993.
- [55] Mohit Prabhushankar and Ghassan AlRegib, “Contrastive reasoning in neural networks,” *arXiv preprint arXiv:2103.12329*, 2021.
- [56] Jonathan Krause, Michael Stark, Jia Deng, and Li Fei-Fei, “3d object representations for fine-grained categorization,” in *4th International IEEE Workshop on 3D Representation and Recognition (3dRR-13)*, Sydney, Australia, 2013.
- [57] Yazeed Alaudah, Motaz Alfarraj, and Ghassan AlRegib, “Structure label prediction using similarity-based retrieval and weakly supervised label mapping,” *Geophysics*, vol. 84, no. 1, pp. V67–V79, 2018.
- [58] Muhammad A Shafiq, Mohit Prabhushankar, Haibin Di, and Ghassan AlRegib, “Towards understanding common features between natural and seismic images,” in *SEG Technical Program Expanded Abstracts 2018*, pp. 2076–2080. Society of Exploration Geophysicists, 2018.
- [59] Xingchao Peng, Ben Usman, Neela Kaushik, Judy Hoffman, Dequan Wang, and Kate Saenko, “Visda: The visual domain adaptation challenge,” *arXiv preprint arXiv:1710.06924*, 2017.
- [60] N. Ponomarenko, O. Ieremeiev, V. Lukin, K. Egiazarian, and M. Carli, “Modified image visual quality metrics for contrast change and mean shift accounting,” in *Proc. CADSM*, 2011, pp. 305–311.
- [61] Z. Wang and Q. Li, “Information content weighting for perceptual image quality assessment,” *IEEE Trans. Image Proc.*, vol. 20, no. 5, pp. 1185–1198, 2011.
- [62] L. Zhang and H. Li, “SR-SIM: A fast and high performance iqa index based on spectral residual,” in *IEEE Int. Conf. Image Proc.*, 2012, pp. 1473–1476.
- [63] L. Zhang, L. Zhang, X. Mou, D. Zhang, et al., “Fsim: a feature similarity index for image quality assessment,” *IEEE Trans. Image Proc.*, vol. 20, no. 8, pp. 2378–2386, 2011.
- [64] D. Temel and G. AlRegib, “PerSIM: Multi-resolution image quality assessment in the perceptually uniform color domain,” in *IEEE Int. Conf. Image Proc.*, 2015, pp. 1682–1686.

- [65] D. Temel and G. AlRegib, “CSV: Image quality assessment based on color, structure, and visual system,” *Sig. Proc.: Image Comm.*, vol. 48, pp. 92 – 103, 2016.
- [66] D. Temel and G. AlRegib, “Perceptual image quality assessment through spectral analysis of error representations,” *Sig. Proc.: Image Comm.*, 2019.
- [67] Mohit Prabhushankar, Dogancan Temel, and Ghassan AlRegib, “Generating adaptive and robust filter sets using an unsupervised learning framework,” in *2017 IEEE International Conference on Image Processing (ICIP)*. IEEE, 2017, pp. 3041–3045.
- [68] Mohit Prabhushankar, Dogancan Temel, and Ghassan AlRegib, “Ms-unique: Multi-model and sharpness-weighted unsupervised image quality estimation,” *Electronic Imaging*, vol. 2017, no. 12, pp. 30–35, 2017.
- [69] Dinesh Jayaraman, Anish Mittal, Anush K Moorthy, and Alan C Bovik, “Objective quality assessment of multiply distorted images,” in *2012 Conference record of the forty sixth asilomar conference on signals, systems and computers (ASILOMAR)*. IEEE, 2012, pp. 1693–1697.
- [70] Nikolay Ponomarenko, Lina Jin, Oleg Jeremeiev, Vladimir Lukin, Karen Egiazarian, Jaakko Astola, Benoit Vozel, Kacem Chehdi, Marco Carli, Federica Battisti, et al., “Image database tid2013: Peculiarities, results and perspectives,” *Signal processing: Image communication*, vol. 30, pp. 57–77, 2015.
- [71] Moloud Abdar, Farhad Pourpanah, Sadiq Hussain, Dana Rezazadegan, Li Liu, Mohammad Ghavamzadeh, Paul Fieguth, Xiaochun Cao, Abbas Khosravi, U Rajendra Acharya, et al., “A review of uncertainty quantification in deep learning: Techniques, applications and challenges,” *Information Fusion*, vol. 76, pp. 243–297, 2021.
- [72] Yarin Gal and Zoubin Ghahramani, “Dropout as a bayesian approximation: Representing model uncertainty in deep learning,” in *international conference on machine learning*. PMLR, 2016, pp. 1050–1059.
- [73] Durk P Kingma, Tim Salimans, and Max Welling, “Variational dropout and the local reparameterization trick,” *Advances in neural information processing systems*, vol. 28, 2015.
- [74] Dequan Wang, Evan Shelhamer, Shaoteng Liu, Bruno Olshausen, and Trevor Darrell, “Tent: Fully test-time adaptation by entropy minimization,” *arXiv preprint arXiv:2006.10726*, 2020.

## Checklist

1. For all authors...
  - (a) Do the main claims made in the abstract and introduction accurately reflect the paper’s contributions and scope? [\[Yes\]](#)
  - (b) Did you describe the limitations of your work? [\[Yes\]](#) . See Section 7.
  - (c) Did you discuss any potential negative societal impacts of your work? [\[Yes\]](#) . See Section 7.
  - (d) Have you read the ethics review guidelines and ensured that your paper conforms to them? [\[Yes\]](#)
2. If you are including theoretical results...
  - (a) Did you state the full set of assumptions of all theoretical results? [\[Yes\]](#)
  - (b) Did you include complete proofs of all theoretical results? [\[Yes\]](#) . See Appendix B
3. If you ran experiments...
  - (a) Did you include the code, data, and instructions needed to reproduce the main experimental results (either in the supplemental material or as a URL)? [\[No\]](#) . The code will be made public upon acceptance.
  - (b) Did you specify all the training details (e.g., data splits, hyperparameters, how they were chosen)? [\[Yes\]](#) . See Section 6 and Appendix C.1
  - (c) Did you report error bars (e.g., with respect to the random seed after running experiments multiple times)? [\[Yes\]](#) . See Appendix D
  - (d) Did you include the total amount of compute and the type of resources used (e.g., type of GPUs, internal cluster, or cloud provider)? [\[Yes\]](#) in Appendix E

4. If you are using existing assets (e.g., code, data, models) or curating/releasing new assets...
  - (a) If your work uses existing assets, did you cite the creators? [Yes] . See Appendix E
  - (b) Did you mention the license of the assets? [Yes] . See Appendix E
  - (c) Did you include any new assets either in the supplemental material or as a URL? [No]
  - (d) Did you discuss whether and how consent was obtained from people whose data you're using/curating? [No]
  - (e) Did you discuss whether the data you are using/curating contains personally identifiable information or offensive content? [No]
5. If you used crowdsourcing or conducted research with human subjects...
  - (a) Did you include the full text of instructions given to participants and screenshots, if applicable? [N/A]
  - (b) Did you describe any potential participant risks, with links to Institutional Review Board (IRB) approvals, if applicable? [N/A]
  - (c) Did you include the estimated hourly wage paid to participants and the total amount spent on participant compensation? [N/A]



## A Appendix : Introspection, Reasoning, and Explanations

Introspection was formalized by [51] as a field in psychology to understand the concepts of memory, feeling, and volition [52]. The primary focus of introspection is in reflecting on oneself through directed questions. While the directed questions are an open field of study in psychology, we use reasoning as a means of questions in this paper. Specifically, abductive reasoning. Abductive reasoning was introduced by the philosopher Charles Sanders Peirce [53], who saw abduction as a reasoning process from effect to cause [54]. An abductive reasoning framework creates a hypothesis and tests its validity without considering the cause. From the perspective of introspection, a hypothesis can be considered as an answer to one of the three following questions: a correlation ‘Why  $P$ ?’ question, a counterfactual ‘What if?’ question, and a contrastive ‘Why  $P$ , rather than  $Q$ ?’ question. Here  $P$  is the prediction and  $Q$  is any contrast class. Both the correlation and counterfactual questions require active interventions for answers. These questions try to assess the causality of some endogenous or exogenous variable and require interventions that are long, complex, and sometimes incomplete [55]. However, introspection is the assessment of ones own notions rather than an external variable. Hence, a contrastive question of the form ‘Why  $P$ , rather than  $Q$ ?’ lends itself as the directed question for introspection. Here  $Q$  is the introspective class. It has the additional advantage that the network  $f(\cdot)$  serves as the knowledge base of notions. All reflection images from 1, Fig. 6, and Fig. 2 are contrastive. We describe the generation process of these *post-hoc* explanations.

**Introspective Feature Visualization** We modify Grad-CAM [6] to visualize  $r_j$  from Eq. 2. Grad-CAM visually justifies the decision made by  $f(\cdot)$  by highlighting features that lead to  $\hat{y}$ . It does so by backpropagating the logit associated with the prediction,  $\hat{y}$ . The resulting gradients at every feature map are global average pooled and used as importance scores. The importance scores multiply the activations of the final convolutional layer and the resultant map is the Grad-CAM visualization. Hence, gradients highlight the activation areas that maximally lead to the prediction  $\hat{y}$ . In Fig. 1, given a spoonbill image  $x$  and a ImageNet-pretrained [23] VGG-16 network, the sensing visualization shown is Grad-CAM. Grad-CAM indicates that the pink and round body, and straight beak are the reasons for the decision. Instead of backpropagating the  $\hat{y}$  logit, we backpropagate  $J(y_I, \hat{y})$  in the Grad-CAM framework. The gradients represent introspective features and are used as importance scores. It can be seen that they visually highlight the explanations to ‘Why  $\hat{y}$ , rather than  $y_I$ ’. In Fig. 1, the network highlights the neck of the spoonbill to indicate that since an S-shaped neck is not observed,  $x$  cannot be a flamingo. Similarly, the body of the spoonbill is highlighted when asked why  $x$  is not a crane since cranes have white feathers while spoonbills are pink. Two more examples are shown in Fig. 6. In the first row, a VGG-16 architecture is trained on Stanford Cars dataset [56]. Given a Bugatti convertible image, Grad-CAM highlights the bonnet as the classifying factor. An introspective question of why it cannot be a bugatti coupe is answered by highlighting the open top of the convertible. The entire car is highlighted to differentiate the bugatti convertible from a Volvo. In the second row, we explore visual explanations in computed seismic images using LANDMASS dataset [57]. A ResNet-18 architecture using the procedure from [58] is trained. The dataset has four geological features as classes - faults, salt domes, horizons, and chaotic regions. Given a fault image in Fig. 6, Grad-CAM highlights the regions where the faults are clearly visible as fractures between rocks. However, these regions resemble salt domes as shown in the representative image. The introspective answer of why  $x$  is not predicted as a salt dome tracks a fault instead of highlighting a general region that also resembles a salt dome. Note that no representative images are required to obtain introspective visualizations. The gradients introspect based on notions of classes in network parameters.

**Biological plausibility of introspection in recognition** Recognition is fast and mostly a feed-forward process. However, when there is uncertainty involved - either due to distributional shift or noise - we tend to reason about our decisions. Human visual system detects salient portions of an image and attends to them in a feed-forward process. An alternative perspective to this is expectancy-mismatch - the idea that HVS attends to those features that deviate from expectations [15]. We simulate this via introspection. By asking ‘Why  $P$ , rather than  $Q$ ?’, we ask the network to examine its expectations and describe the mismatches. This is seen as the lack of S-shaped neck in spoonbill in Fig. 1. By interpreting introspective features as hypotheses that answer contrastive questions, we convert the biologically feed-forward process into a reflection process. Moreover, our results also support this - when train and testsets are from the same distribution, there is no change in results. However, when there is a distributional difference, we notice the gains for introspection - on

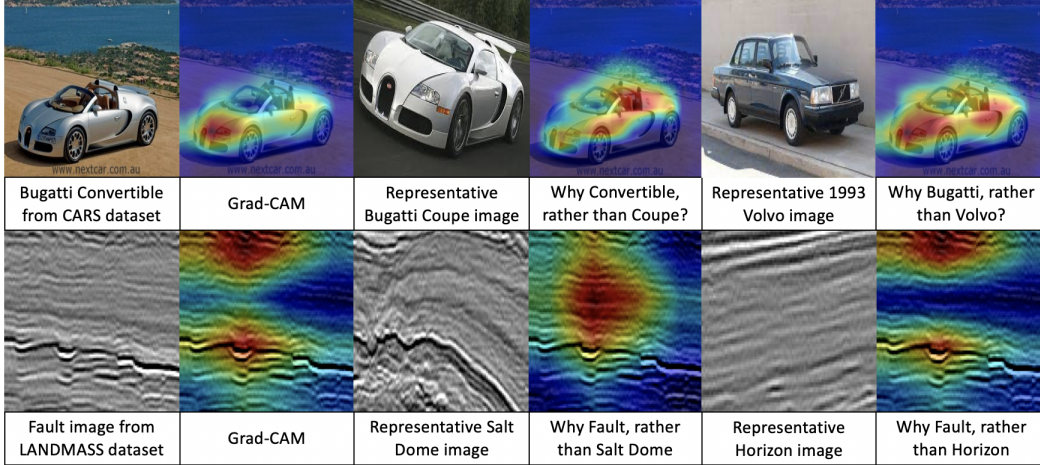


Figure 6: Introspective feature visualizations. The images in the leftmost column are the input  $x$ . The representative images are for illustrative purposes and are not used to extract features.

CIFAR-10C, CIFAR-10-CURE, active learning, OOD and IQA experiments. Moreover, higher the distributional difference, larger is the introspective gain as shown in Fig. 8.

**A broader view on Introspection** In this paper, we limit introspection as answers to ‘*Why  $P$ , rather than  $Q$ ?*’ questions. We limit  $P$  to be the predictions made by networks. Hence, we are left with  $N$  questions to answer. However, creative abduction calls for asking questions of the form ‘*Why  $P$ , rather than  $Q1$  and  $Q2$ ?*’. Such  $Qs$  can extend to all  $N$  classes. Hence, introspective labels can be the powerset of all one-hot labels -  $2^N$ . Moreover, the prediction itself can be made to change by intervening within data leading to questions of the form ‘*Why  $Q$ , rather than  $P$ ?*’. These include counterfactual questions of the form ‘*What if?*’ when considered from the output perspective. Hence, for  $N$  classes, there can be  $N \times 2^N$  introspective questions. Hence, the proposed features are only one possible feature set when considering introspection. However, we posit that all these features are a function of the data and the model, thereby making gradients an essential feature set while considering introspection and this paper provides intuitions as to their applicability.

## B Appendix : Proofs

### B.1 Proof for Lemma 1

We start by assuming  $J(\cdot)$  is a cross-entropy loss.  $J(y_I, \hat{y}), I \in [1, N]$  can also be written as,

$$J(y_I, \hat{y}) = -y_{\hat{y}} + \log \sum_{j=1}^N e^{y_j}, \text{ where } \hat{y} = f(x), \hat{y} \in \mathbb{R}^{N \times 1}. \quad (12)$$

This definition is used in PyTorch to implement cross entropy. Here we assume that the predicted logit, i.e, the argument of the max value in the logits  $\hat{y}$  is  $y_{\hat{y}}$ . While training,  $y_{\hat{y}}$  is the true label. In this paper, we backpropagate any trained class  $I$ , as an introspective class. Hence, Eq. 12 can be rewritten as,

$$J(y_I, \hat{y}) = -y_I + \log \sum_{j=1}^N e^{y_j}, \text{ where } \hat{y} = f(x), \hat{y} \in \mathbb{R}^{N \times 1}. \quad (13)$$

Approximating the exponent within the summation with its second order Taylor series expansion, we have,

$$J(y_I, \hat{y}) = -y_I + \log \sum_{j=1}^N \left( 1 + y_j + \frac{y_j^2}{2} \right). \quad (14)$$

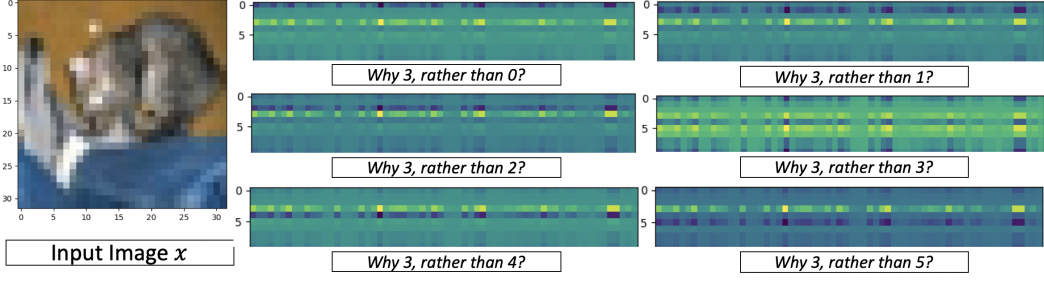


Figure 7: For the input image on the left, the  $\nabla_{W_L} J(y_I, 3)$  are shown on the right. Each image is a visualization of the  $64 \times 10$  gradient matrix.

Note that for a well trained network  $f(\cdot)$ , the logits of all but the predicted class are negligible. As noted before, the predicted logit is  $y_{\hat{y}}$ . Taking  $y_{\hat{y}}$  within the summation as common,

$$J(y_I, \hat{y}) = -y_I + \log \sum_{j=1}^N y_{\hat{y}} \left( \frac{1}{y_{\hat{y}}} + \frac{y_j}{y_{\hat{y}}} + \frac{y_j^2}{2y_{\hat{y}}} \right). \quad (15)$$

Taking out  $y_{\hat{y}}$  from within the summation since it is a constant and independent of summation variable  $j$ ,

$$J(y_I, \hat{y}) = -y_I + \log \left( y_{\hat{y}} \sum_{j=1}^N \left( \frac{1}{y_{\hat{y}}} + \frac{y_j}{y_{\hat{y}}} + \frac{y_j^2}{2y_{\hat{y}}} \right) \right). \quad (16)$$

Using product rule of logarithms,

$$J(y_I, \hat{y}) = -y_I + \log(y_{\hat{y}}) + \log \sum_{j=1}^N \left( \frac{1}{y_{\hat{y}}} + \frac{y_j}{y_{\hat{y}}} + \frac{y_j^2}{2y_{\hat{y}}} \right). \quad (17)$$

For a well trained network, all logits except  $y_{\hat{y}}$  are negligible. Also for a well trained network,  $y_{\hat{y}}$  is large. Hence the third term on the RHS within the summation reduces to  $1 + \frac{y_{\hat{y}}}{2}$ . Note that in the second term of the RHS,  $y_{\hat{y}} = c$  is a constant for any deterministic trained network even when there are small changes in the values of weights  $W$ . Substituting,

$$J(y_I, \hat{y}) = -y_I + \log(c) + \log \left( 1 + \frac{y_{\hat{y}}}{2} \right). \quad (18)$$

The quantity in Eq. 18 is differentiated, hence nulling the effect of constant  $\log(c)$ . Hence, we can obtain  $\nabla_W J(y_I, \hat{y})$  as a function of two logits,  $y_I$  and  $y_{\hat{y}}$  given by,

$$\nabla_W J(y_I, \hat{y}) = -\nabla_W y_I + \nabla_W \log \left( 1 + \frac{y_{\hat{y}}}{2} \right). \quad (19)$$

$y_I$  is a one-hot vector of dimensionality  $N \times 1$  while  $\nabla_W$  is a  $d_{L-1} \times N$  matrix. The product extracts only the  $I^{th}$  filter in the  $W$  matrix in gradient calculations. Following the above logic for  $y_{\hat{y}}$ , we have,

$$\nabla_W J(y_I, \hat{y}) = -\nabla_{W_I} y_I + \nabla_{W, y_{\hat{y}}} g(y_{\hat{y}}), \quad (20)$$

where  $g(\cdot)$  is some function of  $y_{\hat{y}}$ . Hence the gradient  $r_I = \nabla_W J(y_I, \hat{y})$  lies in the span of the filter gradients of  $W_I$  and  $W_{\hat{y}}$ , making  $r_I$  orthogonal to all other filter gradient pairs. Hence proven.

Hence, for  $N$  introspective features in 5, the space complexity of  $r_x$  which is a concatenation of  $N$  separate  $r_i$ , reduces from  $\mathcal{O}(d_{L-1} \times N^2)$  to  $\mathcal{O}(d_{L-1} \times N)$ .

Similar to Fig. 2 that was presented on a well trained network on MNIST dataset, we show the sparsity analysis on CIFAR-10 data in Fig. 7. The sparse nature of gradients is still observed in Fig. 7 but it is not as prevalent as the gradients from Fig. 2. This is because of the assumption of the well trained network in Lemma 1. This assumption allows for Eq. 18 where we assume only the predicted logit and its closest logit are non-zero. However, in Table 9, we show that the approximation does not alter the empirical results since the excess non-zero logits tend to store redundant information across filters. This is also observable in Fig. 7.

Table 4: Structure of  $\mathcal{H}(\cdot)$  and accuracies on CIFAR-10C as reported in the paper.

(Training Domain) $f(\cdot)$	Part 1: Structure of $\mathcal{H}(\cdot)$ - All layers separated by sigmoid	Accuracy (%)
(CIFAR-10) R-18,34	$640 \times 300 - 300 \times 100 - 100 \times 10$	71.4, 73.36
(CIFAR-10) R-50, 101	$2560 \times 300 - 300 \times 100 - 100 \times 10$	75.2, 75.47
(Webcam) R-18,34	$1984 \times 31$	-
(Webcam) R-50,101	$7936 \times 31$	-
(Amazon) R-18,34	$1984 \times 1000 - 1000 \times 100 - 100 \times 31$	-
(Amazon) R-50,101	$7936 \times 3000 - 3000 \times 500 - 500 \times 31$	-
(DSLR) R-18,34	$1984 \times 1000 - 1000 \times 100 - 100 \times 31$	-
(VisDA) R-18	$768 \times 300 - 300 \times 100 - 100 \times 12$	-

## B.2 Proof for Theorem 1

The proof for Theorem 1 follows from Lemma 1. For any given data  $x$ , there are  $N$  possible introspections and hence  $N$  possible reflections. The LHS in Eq. 20 is summed across  $N$  losses. Since  $y_j, j \in [1, N]$  are one-hot vectors, they are orthogonal and the first term in RHS is an addition across  $j$ . The second term in RHS is independent of  $j$ . Representing this in equation form, we have,

$$\sum_{j=1}^N \nabla_W J(y_j, \hat{y}) = - \sum_{j=1}^N \nabla_{W,j} y_j + N \times \nabla_{W,y_{\hat{y}}} g(y_{\hat{y}}). \quad (21)$$

The first term is added  $N$  times for  $N$  orthogonal  $y_j$ . Hence, the first term reduces to a sum of all gradients of  $j^{th}$  filters when backpropagating  $y_j$ . Removing the summation and replacing  $y_j = \mathbf{1}_N$  or a vector of all ones in the LHS, we still have the same RHS given by,

$$\nabla_W J(\mathbf{1}_N, \hat{y}) = - \sum_{j=1}^N \nabla_{W,j} y_j + N \times \nabla_{W,y_{\hat{y}}} g(y_{\hat{y}}). \quad (22)$$

Equating the LHS from Eq. 21 and Eq. 22, we have the proof.

## B.3 Tradeoff in Eq. 8

Eq. 8 suggests a trade-off between minimizing  $\mathbb{E}[(\mathcal{H}(r_x) - y)^2]$ , which is the cost function for training  $\mathcal{H}(\cdot)$ , and the variance of the network  $\mathcal{H}(\cdot)$ . Ideally, an optimal point exists that optimally minimizes the cost function of  $\mathcal{H}(\cdot)$  while maximizing its variance. This also prevents decomposing  $\mathcal{H}(\cdot)$  into  $\mathcal{H}_1(\cdot)$  and  $\mathcal{H}_2(\cdot)$  that further introspect on  $\mathcal{H}(\cdot)$ . In this paper, we create a single introspective network  $\mathcal{H}(\cdot)$ . Hence, we do not comment further on the practical nature of the trade-off or perpetual introspection. It is currently beyond the scope of this work. In all experiments, we train  $\mathcal{H}(\cdot)$  as any other network feed-forward network - by minimizing an empirical loss function given the ground truth.

## B.4 Fisher Vector Interpretation

We make two claims before Eq. 10 both of which are well established. These include :

- **Variance of a linear function** For a linear function  $y = W \times x + b$ , the variance of  $y$  is given by  $\text{Var}(Wx + b) = W^2 \text{Var}(x)$  if  $\text{Var}(W) = 0$ .
- **Variance of a linear function when  $W$  is estimated by gradient descent** Ignoring the bias  $b$ , and taking  $y = Wx = x^T \Sigma^{-1} x^T (xW)$ , we have  $\text{Var}(Wx) = \sigma^2 \text{Tr}(x^T \Sigma^{-1} x)$ .

Both these results lead to Eq. 9. Since  $r_x \in \mathfrak{R}^{d_L - 1 \times N}$ , the trace of the matrix given by  $\text{Tr}(r_x^T F^{-1} r_x)$ , is a sum of projections on individual weight gradients given by  $\sum_{j=1}^N r_j^T F^{-1} r_j$  in the Fisher sense.

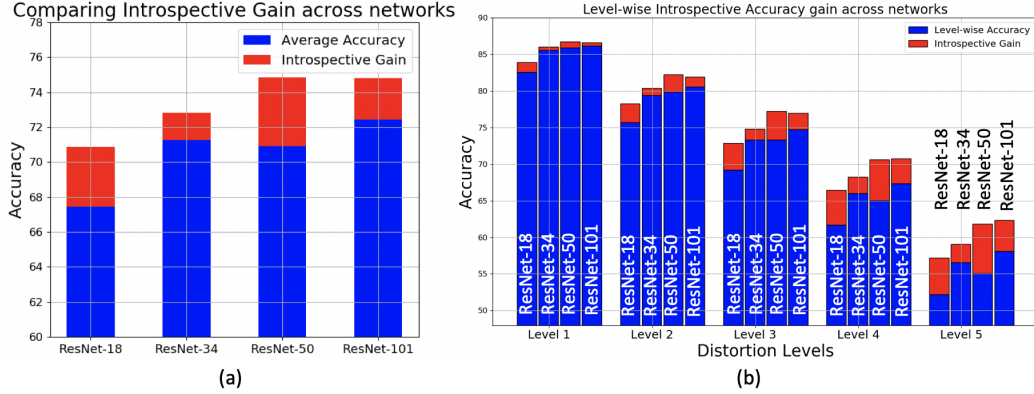


Figure 8: Introspective performance gains over Feed-Forward networks of a) ResNets-18,34,50,101, b) Level-wise averaged results across ResNets-18,34,50,101

## C Appendix : Additional Results on Recognition and Calibration

### C.1 Structure of $\mathcal{H}(\cdot)$ and training details

In this section, we provide the structure of the proposed  $\mathcal{H}(\cdot)$  architecture. Note that, from Eq. 1, the  $y_{feat}$  in feed-forward learning are processed through a linear layer. We process the introspective features  $r_x$  through an MLP  $\mathcal{H}(\cdot)$ , whose parameter structure is given in Table 4. Hence, we follow the same workflow as feed-forward networks in introspective learning. The feed-forward features  $f_{L-1}(x)$  are passed through the last linear layer in  $f(\cdot)$  to obtain the prediction  $\hat{y}$ . The introspective features are passed through an MLP to obtain the prediction  $\tilde{y}$ . The exact training procedure for  $\mathcal{H}(\cdot)$  is presented below.

**Training  $f(\cdot)$  and Hyperparameters** We train four ResNet architectures - ResNet-18, 34, 50, and 101 [4]. Note that we are not using any known techniques that promote either generalization (training on noisy data [28]) or calibration (Temperature scaling [37]). The networks are trained from scratch on CIFAR-10 dataset which consists of 50000 training images with 10 classes. The networks are trained for 200 epochs using SGD optimizer with momentum = 0.9 and weight decay =  $5e-4$ . The learning rate starts at 0.1 and is changed as 0.02, 0.004, 0.0008 after epochs 60, 120, and 160 respectively. PyTorch in-built Random Horizontal Flip and standard CIFAR-10 normalization is used as preprocessing transforms.

**Training  $\mathcal{H}(\cdot)$**  The structures of all MLPs are shown in Table 4. ResNet-18,34 trained on CIFAR-10 provide  $r_x$  of dimensionality  $640 \times 1$ . This is fed into  $\mathcal{H}(\cdot)$  which is trained to produce a  $10 \times 1$  output. Note that  $r_x$  from ResNet-50,101 are of dimensionality  $2560 \times 1$  - due to larger dimension of  $f_{L-1}(\cdot)$ . All MLPs are trained similar to  $f(\cdot)$  - for 200 epochs, SGD optimizer, momentum = 0.9, weight decay =  $5e-3$ , learning rates of 0.1, 0.02, 0.004, 0.0008 in epochs 1 – 60, 61 – 120, 121 – 160, 161 – 200 respectively. For the larger 5-layered ResNet-50,101 networks in Table 9, dropout with 0.1 is used and the weight decay is reduced to  $5e-4$ .

### C.2 Introspective Accuracy Gain and Calibration Error Studies

In this section, we present additional recognition and calibration results. In Fig. 5a), we showed distortion-wise accuracy and the introspective gain for ResNet-18. In this section, we present level-wise and network-wise accuracies for all four considered ResNet architectures. We show that an introspective ResNet-18 matches a Feed-Forward ResNet-50 in terms of recognition performance. We then compare the results of ResNet-18 against existing techniques that promote robustness. We show that introspection is a plug-in approach that acts on top of existing methods and provides gain. We do the same for calibration experiments on CIFAR-10C where we provide level-wise distortion-wise graphs for Expected Calibration Error (ECE) similar to Fig. 5b).

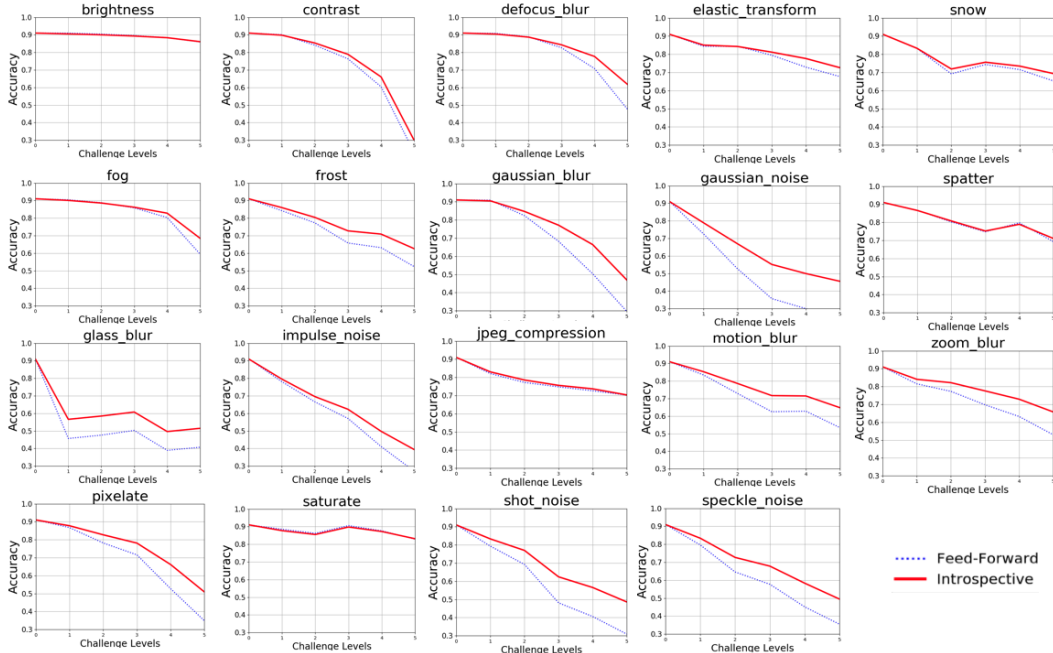


Figure 9: Introspective performance gains over Feed-Forward Resnet-18 across distortions and levels

### C.2.1 Level-wise Recognition on CIFAR-10C

In Fig. 8b), the introspective performance gains for the four networks are categorized based on the distortion levels. All 19 categories of distortion on CIFAR-10C are averaged for each level and their respective feed-forward accuracy and introspective gains are shown. Note that the levels are progressively more distorted. Hence, level 1 distribution  $\mathcal{X}'$  is similar to the training distribution  $\mathcal{X}$  when compared to level 5 distributions. As the distortion level increases, the introspective gains also increase. This is similar to the results from Section D. In both active learning and OOD applications as  $\mathcal{X}'$  deviates from  $\mathcal{X}$ , introspection performs better. In Fig. 8a), we show the distortion-wise and level-wise increase for each network. Note that, an Introspective ResNet-18 performs similarly to a Feed-Forward ResNet-50. From [4], the number of parameters in a ResNet-18 model ( $1.8 \times 10^9$ ) are less than half the parameters in a ResNet-50 model ( $3.8 \times 10^9$ ). However by adding an introspective model  $\mathcal{H}(\cdot)$  with  $2.23 \times 10^5$  parameters to a feed-forward ResNet-18 model, we can obtain the same accuracy as a ResNet-50 model. This is in addition to the calibration gains provided by introspection.

### C.2.2 Distortion-wise and Level-wise Recognition on CIFAR-10C

In Fig. 9, the introspective accuracy performance for Resnet-18 across 19 distortions and 5 distortion levels is shown. Note that CIFAR-10C consists of 950,000 test images. The 4% increase in performance translates to around 35,000 more images correctly classified over its feed-forward counterpart. These gains are especially visible among Level 5 distortions.

Table 5: Introspecting on top of existing robustness techniques.

Methods	Accuracy
ResNet-18	67.89%
Denosing	65.02%
Adversarial Train [27]	68.02%
SimCLR [19]	70.28%
Augment Noise [28]	76.86%
Augmix [26]	89.85%
ResNet-18 + Introspection	71.4%
Denosing + Introspection	68.86%
Adversarial + Introspection	70.86%
SimCLR + Introspection	73.32%
Augment Noise + Introspection	77.98%
Augmix + Introspection	89.89% (ECE 43.33% ↓)

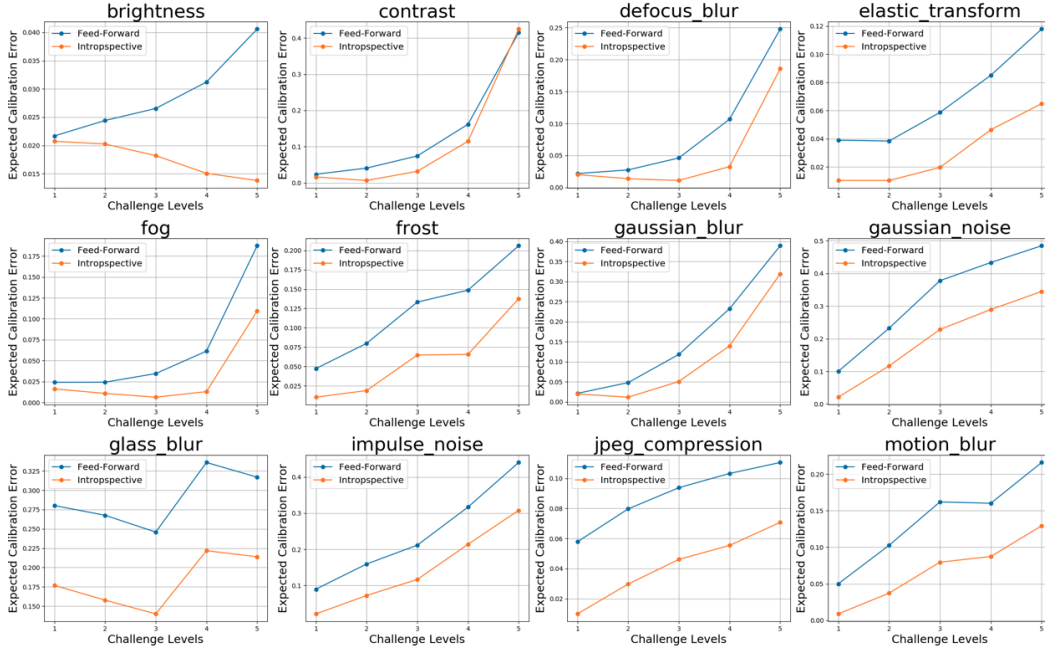


Figure 10: ECE vs distortion levels across 12 separate distortions from CIFAR-10C for ResNet-18.

### C.2.3 Introspection as a plug-in on top of existing techniques

Several techniques exist that boost the robustness of neural networks to distortions. These include training with noisy images [28], training with adversarial images [27], and self-supervised methods like SimCLR [19] that train by augmenting distortions. Another commonly used technique is to pre-process the noisy images to denoise them. All these techniques can be used to train  $f(\cdot)$ . Our proposed framework sits on top of any  $f(\cdot)$ . Hence, it can be used as a plug-in network. These results are shown in Table 5. Denoising 19 distortions is not a viable strategy assuming that the characteristics of the distortions are unknown. We use Non-Local Means denoising and the results obtained are lower than the feed-forward accuracy by almost 3%. However, introspecting on this model increases the results by 3.84%. We create untargeted adversarial images using I-FGSM attack with  $\alpha = 0.01$  and use them to train a ResNet-18 architecture. In our experiments this did not increase the feed-forward accuracy. Introspecting on this network provides a gain of 2.84%. SimCLR [19] and introspection on SimCLR is discussed in Section C.3. In the final experimental setup of augmenting noise [28], we augment the training data of CIFAR-10 with six distortions - gaussian blur, salt and pepper, gaussian noise, overexposure, motion blur, and underexposure - to train a ResNet-18 network  $f'(\cdot)$ . We use the noise characteristics provided by [40] to randomly distort 500 CIFAR-10 training images by each of the six distortions. The original training set is augmented with the noisy data and trained. The results of the feed-forward  $f'(\cdot)$  show a substantial increase in performance to 76.86%. This is about 9% increase from the original architecture. We show that introspecting on  $f'(\cdot)$  provides a further gain in accuracy of 1.12%. Note that to train  $\mathcal{H}(\cdot)$ , we do not use the augmented data. We only use the original CIFAR-10 undistorted training set. The gain obtained is by introspecting on only the undistorted data, even though  $f'(\cdot)$  contains knowledge of the distorted data. Hence, introspection is a plug-in approach that works on top of any network  $f(\cdot)$  or enhanced network  $f'(\cdot)$ . Augmix [26] is currently the best performing technique on CIFAR-10C. It creates multiple chains of augmentations to train the base WideResNet network. On CIFAR-10C,  $f'(\cdot)$  obtains 89.85% recognition accuracy. We use  $f'(\cdot)$  as our base sensing model and train an introspective MLP on  $f'(\cdot)$ . Note that we do not use any augmentations for training  $\mathcal{H}(\cdot)$ . Doing so, we obtain a statistically similar accuracy performance of 89.89%. However, the expected calibration error of the feed-forward  $f'(\cdot)$  model decreases by 43.33% after introspection. Hence, when there is no accuracy gains to be had, introspection provides calibrated models.

Table 6: Expected Calibration Error and Maximum Calibrated Error for Feed-Forward vs Introspective Networks.

Architectures		ResNet-18	ResNet-34	ResNet-50	ResNet-101
ECE ( $\downarrow$ )	$f(\cdot)$	0.14	0.18	0.13	0.16
	$\mathcal{H}(\cdot)$	<b>0.07</b>	<b>0.09</b>	<b>0.06</b>	<b>0.1</b>
MCE ( $\downarrow$ )	$f(\cdot)$	0.27	0.34	0.27	0.32
	$\mathcal{H}(\cdot)$	<b>0.23</b>	<b>0.24</b>	<b>0.25</b>	<b>0.23</b>

### C.2.4 Expected Calibration Error (ECE)

In Fig. 5b), we show ECE for two distortion types - brightness and saturation across 5 distortion levels. In Fig. 10, we show results across five distortion levels for the first 12 distortions. The blue plot is the Feed-Forward ECE while the lower orange plot is its introspective counterpart. Apart from Level 5 contrast, introspective ResNet-18 is more calibrated than its feed-forward counterpart. This is in addition to the performance gains. The trend remains the same in the remaining distortions and among all considered networks. We average out ECE across 19 distortions and 5 challenge levels and provide ECE results for ResNets-18, 34, 50, 101 in Table 6. Lower the error, better is the architecture. The proposed introspective framework decreases the ECE of its feed-forward backbone by approximately 42%. An additional metric called Maximum Calibration Error (MCE) is also used for comparison. While ECE averages out the calibration difference in all bins (From Section 6), MCE takes the maximum error among all bins [37]. The introspective networks outperform their feed-forward backbones among all architectures when compared using ECE and MCE.

Table 7: SimCLR and its supervised and introspective variations tested on CIFAR-10C.

Methods	ResNet-18	ResNet-34	ResNet-50	ResNet-101
SimCLR [19]	70.28%	69.5%	67.32%	64.68%
SimCLR-MLP	72.79%	72.54%	70.37%	70.89%
SimCLR-Introspective (Proposed)	<b>73.32%</b>	<b>73.06%</b>	<b>71.28%</b>	<b>71.76%</b>

### C.3 SimCLR and Introspection

SimCLR [19] is a self-supervised contrastive learning framework that is robust to noise distortions. The algorithm involves creating augmentations of existing data including blur, noise, rotations, and jitters. The network is made to contrast between all the augmentations of the image and other images in the batch. A separate network head  $g(\cdot)$  is placed on top of the network to extract features and inference is made by creating a similarity matrix to a feature bank. Note that  $g(\cdot)$  is a simple MLP. Our proposed framework is similar to SimCLR in that we extract features and use an MLP  $\mathcal{H}(\cdot)$  to infer from these features. In Table 5, we show the results of Introspecting ResNets against SimCLR. However, this comparison is unfair since the features in SimCLR are trained in a self-supervised fashion. In this section, we train SimCLR for ResNets-18, 34, 50, 101 and train a new MLP  $g(\cdot)$ , not for extracting features, but to classify images. In other words, in [19], the authors create  $g(\cdot)$  to be a  $512 \times 128$  layer that extracts features. We train a network of the form  $512 \times 128 - 128 \times 10$  that is trained to classify images. We then introspect on this  $g(\cdot)$  to obtain  $r_x$ . Hence, our extracted features are a result of introspecting on self-supervision. Note that  $g(\cdot)$  is now a fully supervised network. We pass CIFAR-10C through  $g(\cdot)$  and name it SimCLR-MLP in Table 7. It is unsurprising that the fully-supervised SimCLR-MLP beats the self-supervised SimCLR across all four ResNets. The introspective network is called SimCLR-Introspective in Table 7. Note that there is less than 1% recognition performance increase across networks compared to SimCLR-MLP. Hence, the performance gains for introspecting on SimCLR-MLP is not as high as base ResNet architectures from Table 5. One hypothesis for this marginal increase is that the notions created within SimCLR-MLP are predominantly from the self-supervised features in SimCLR. These may not be amenable for the current framework of introspection that learns to contrast between classes and not between features within-classes.

### C.4 Ablation Studies

The feature generation process in Section 2 is dependent on the loss function  $J(\hat{y}, y)$ . In this section, we analyze the performance of our framework for commonly used loss functions and show that the



Table 8: Introspective Learning accuracies when  $r_x$  is extracted with different loss functions for ResNet-18 on CIFAR-10C.

Feed-Forward	MSE-M	CE	BCE	L1	L1-M	Smooth L1	Smooth L1-M	NLL	SoftMargin
67.89%	<b>71.4%</b>	69.47%	70.76%	70.12%	70.72%	70.42%	70.63%	70.93%	70.91%

Table 9: Ablation studies for  $\mathcal{H}(\cdot)$  on CIFAR-10C.

<b>Part 1 : Varying the number of layers</b>		
R-18	Feed-Forward $64 \times 10$	67.89%
	$640 \times 10$	71%
	$640 \times 100 - 100 \times 10$	<b>71.57%</b>
	$640 \times 300 - 300 \times 100 - 100 \times 10$	71.4%
	$640 \times 400 - 400 \times 200 - 200 \times 100 - 100 \times 10$	66.1%
R-50	Feed-Forward $64 \times 10$	71.8%
	$2560 \times 300 - 300 \times 100 - 100 \times 10$	<b>75.2%</b>
	$2560 \times 1000 - 1000 \times 500 - 500 \times 300 - 300 \times 100 - 100 \times 10$	73%
<b>Part 2 : Is the performance increase only because of a large <math>\mathcal{H}(\cdot)</math>?</b>		
R-18	Feed-Forward	67.89%
	$f_L(\cdot)$ 1 Layer : $64 \times 10$	67.86%
	$\mathcal{H}(\cdot)$ 1 Layer : $640 \times 10$	<b>71%</b>
	$f_L(\cdot)$ 3 Layers $64 \times 30 - 30 \times 20 - 20 \times 10$	63.61%
	$f_L(\cdot)$ 3 Layers $64 \times 512 - 512 \times 256 - 256 \times 10$	64.78%
	$\mathcal{H}(\cdot)$ 3 Layers: $640 \times 300 - 300 \times 100 - 100 \times 10$	<b>71.4%</b>
	$f_L(\cdot)$ , 6200 parameters : $64 \times 50 - 50 \times 40 - 40 \times 20 - 20 \times 10$	66.85%
	$\mathcal{H}(\cdot)$ , 6400 parameters : $640 \times 10$	<b>71%</b>
	Prediction on $y_{feat}$ using 10-NN (No $f_L(\cdot)$ )	66.31%
	Prediction on $r_x$ using 10-NN (No $\mathcal{H}(\cdot)$ )	<b>68.76%</b>
<b>Part 3 : VGG-16</b>		
VGG-16	Feed-Forward	68.96%
	$f(\cdot)$ $512 \times 1024 - 1024 \times 256 - 256 \times 10$	62.43%
	$\mathcal{H}(\cdot)$ $5120 \times 1000 - 1000 \times 100 - 100 \times 10$	<b>73.79%</b>
<b>Part 4 : Effect of approximation of Lemma 1 and Theorem 1</b>		
R-18	Feed-Forward	$67.89 \pm 0.23\%$
	With Approximation	$71.57 \pm 0.12\%$
	Without Approximation	$71.43 \pm 0.11\%$

introspective network outperforms its feed-forward counterpart under any choice of  $J(\hat{y}, y)$ . We also ascertain the effect of the size of the parameter set in  $\mathcal{H}(\cdot)$  on performance accuracy.

#### C.4.1 Effect of Loss functions

We extract  $r_x$  using 9 loss functions and report the final distortion-wise level-wise averaged results Table 8. We do so for ResNet-18 and for the architecture of  $\mathcal{H}(\cdot)$  shown in Table 4. The following loss functions are compared : CE is Cross Entropy, MSE is Mean Squared Error, L1 is Manhattan distance, Smooth L1 is the leaky extension of Manhattan distance, BCE is Binary Cross Entropy, and NLL is Negative Log Likelihood. Notice that the performance of  $r_x$  extracted using all loss functions exceed that of the feed-forward performance. The shown results of MSE, L1-M and Smooth L1-M are obtained by backpropagating a  $\mathbf{1}_N$  from Theorem 1 vector multiplied by the average of all maximum logits  $M$ , in the training dataset. We use  $M$  instead of 1 because we want the network to be as confident of the introspective label  $y_I$  as it is with the prediction label  $\hat{y}$ . Note that the results in Table 8 are for CIFAR-10C. MSE-M outperforms NLL loss by 0.37% in average accuracy and is used in our experiments.

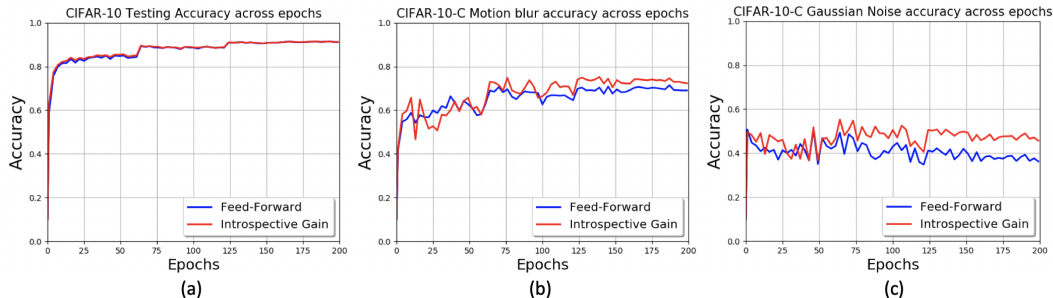


Figure 11: Introspective vs. Feed-Forward accuracy of ResNet-18 across training epochs on (a) CIFAR-10 original testset, (b) CIFAR-10C Motion Blur Testset on all 5 challenge levels, (c) CIFAR-10C Gaussian Noise Testset on all 5 challenge levels.

### C.4.2 Effect of $\mathcal{H}(\cdot)$

We conduct ablation studies to empirically show the following : 1) the design of  $\mathcal{H}(\cdot)$  does not significantly vary the introspective results, 2) the extra parameters in  $\mathcal{H}(\cdot)$  are not the cause of increased performance accuracy.

**How does changing the structure of  $\mathcal{H}(\cdot)$  change the performance?** We vary the architecture of  $\mathcal{H}(\cdot)$  from a single linear layer to 4 layers in the first half of Table 9 for ResNet-18. The results in the first three cases are similar. A four layered network performs worse than  $f(\cdot)$ . However, changing the weight decay from  $5e^{-3}$  to  $5e^{-4}$  during training increases the results to above 70% but does not beat the smaller networks. For ResNet-18 architecture, the highest results are obtained when  $\mathcal{H}(\cdot)$  is a 2-layered architecture but for the sake of uniformity, we use the results from a 3-layered network across all ResNet architectures.

**Are the extra parameters in  $\mathcal{H}(\cdot)$  the only cause for increase in performance accuracy?** We show an ablations study of the effect of structure of  $\mathcal{H}(\cdot)$  and  $f(\cdot)$  on the introspective and feed-forward results in Part 2 of of Table 4 on CIFAR-10-C dataset. The results are divided into four sections. In the first section, we show the performance of the original feed-forward network  $f(\cdot)$ , the performance when the final layer,  $f_L(\cdot)$  is retrained using features  $y_{feat}$  from Eq. 1, and the introspective network when  $\mathcal{H}(\cdot)$  is a single layer. The second section shows the results when the features  $y_{feat}$  are used to train a three layered network  $f_L(\cdot)$ , and the introspective network is also three layered. Finally, in section 3, we try to equate the number of parameters for  $f_L(\cdot)$  and  $\mathcal{H}(\cdot)$ . Note that in all cases,  $f_L(\cdot)$  and  $\mathcal{H}(\cdot)$  are trained in the same manner as detailed in Section C.1.  $\mathcal{H}(\cdot)$  beats the performance of  $f_L(\cdot)$  among all ablation studies. Finally, similar to SimCLR, we forego using an MLP and use 10-Nearest Neighbors on  $y_{feat}$  ( $64 \times 1$ ) and  $r_x$  ( $640 \times 1$ ) for predictions. Both results are worse-off than their MLP results but  $r_x$  outperforms  $y_{feat}$ .

**Introspection on larger  $r_x$  and wider  $f_{L-1}(\cdot)$**  On Resnet-101 experiments in Section C.2.1,  $r_x$  is of dimension  $2560 \times 1$ . On all Resnet-18 experiments,  $r_x$  is  $640 \times 1$ . In part 3 of Table 4, we show results on a larger VGG-16 architecture where  $r_x$  is of size  $5120 \times 1$ . Row 1 shows the normal feed-forward accuracy. Row 3 is the introspective results on VGG-16 and the results are 4.83% higher than its feed-forward counterpart. In row 2, we expand the penultimate layer of  $f(\cdot)$  from 512 to 1024 so as to include more parameters in the feed-forward network. Note that this is not possible for Resnet-18 as  $f_{L-1}(\cdot)$  is  $64 \times 1$ . Hence, we compare our introspective network against a wider  $f(\cdot)$  architecture instead of an elongated architecture like in Part 2. In both cases, introspection outperforms additional parameters in  $f(\cdot)$ .

**Effect of Lemma 1 and Theorem 1** Note that with approximations from Lemma 1 and Theorem 1,  $r_x$  generation occurs with a time complexity of  $\mathcal{O}(1)$ . Without approximation,  $r_x$  generation occurs in  $\mathcal{O}(N)$ . However, the results are statistically insignificant when averaged across 5 seeds.

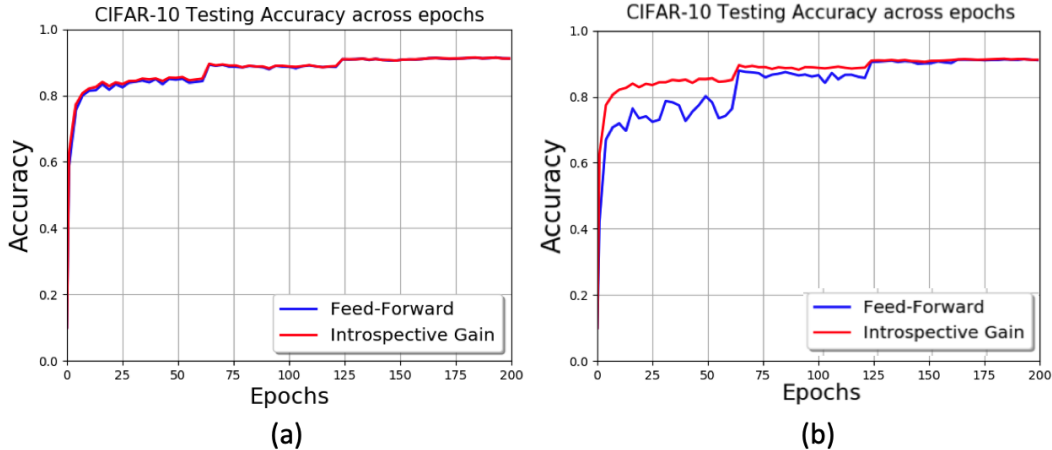


Figure 12: Introspective vs. Feed-Forward accuracy of ResNet-18 across training epochs when (a)  $f(\cdot)$  and  $\mathcal{H}(\cdot)$  are trained on the same training set (b)  $\mathcal{H}(\cdot)$  is trained on a separate held-out validation set

### C.5 Introspective accuracy across training epochs

In Section 2, we make the assumption that  $f(\cdot)$  is well trained to approximate  $r_x$  using Theorem 1. In Section 4, the Fisher Vector analysis works when the gradients form distances across the manifold in  $f(\cdot)$  which occurs if  $f(\cdot)$  is well trained. In this section we show that, practically, introspection performs as well as feed-forward accuracy across training epochs on CIFAR-10 testset and outperforms feed-forward accuracy on CIFAR-10C distortions. We show results on original testset, gaussian noise and motion blur testsets in Fig. 11.

**Training, Testing, and Results in Fig. 11a** In this experimental setup, ResNet-18 is trained for 200 epochs. The model states at multiples of 3 epochs from 1 to 200 are stored. This provides 67 states of  $f(\cdot)$  along its training process. Each  $f(\cdot)$  is tested on CIFAR-10 testset and the recognition accuracy is plotted in blue in Fig. 11a). The introspective features  $r_x$  for all 67 states are extracted for the 50,000 training samples. These  $r_x$  are used to train 67 separate  $\mathcal{H}(\cdot)$  of structure provided in Table 4 with a similar training setup as in Section C.1. The  $r_x$  from the 10,000 testing samples are extracted individually for each of the 67  $f(\cdot)$  states and tested. The results are plotted in red in Fig. 11a). Note the sharp spikes at epochs 60 and 120 where there is a change in the learning rate. Hence, when training and testing distributions are similar, introspective and feed-forward learning provides statistically similar performance across varying states of  $f(\cdot)$ .

**Training, Testing, and Results in Fig. 11b, c** We now consider the case when a network  $f(\cdot)$  is trained on distribution  $\mathcal{X}$  and tested on  $\mathcal{X}'$  from CIFAR-10C distortions. The 67 trained models of ResNet-18 are tested on two distortions from CIFAR-10C. From the results in Fig. 5, introspective learning achieves one of its highest performance gains in Gaussian noise, and an average increase in motion blur after epoch 200. The results in Fig. 11 indicate that after approximately 60 epochs, the feed-forward network has sufficiently sensed notions to reflect between classes. This is seen in the performance gains in both the motion blur and Gaussian noise experiments.

**Training of  $\mathcal{H}$  on a separate validation set in Fig. 12b** In all experiments, the introspective network  $\mathcal{H}(\cdot)$  is trained on the same training set as  $f(\cdot)$ . In Fig. 12, we show the results when the introspective network is trained on a separate portion of the dataset. We use 40,000 images to train  $f(\cdot)$  and 10,000 to train  $\mathcal{H}(\cdot)$  both of which are randomly chosen. We follow the training procedure from before. The model states at multiples of 3 epochs from 1 to 200 are stored. This provides 67 states of  $f(\cdot)$  along its training process. Each  $f(\cdot)$  is tested on CIFAR-10 testset and the recognition accuracy is plotted in blue in Fig. 12b). The  $\mathcal{H}(\cdot)$  at each iteration on the other hand is trained with the 10,000 images. However, it has access to the notions created from the remaining 40,000 images and hence the results for introspection match Fig. 11a) which is reproduced in Fig. 12a). The feed-forward results catch up to the introspective results around epoch 60. At Epoch 120, we add

Table 10: Performance of Proposed Introspective  $\mathcal{H}(\cdot)$  vs Feed-Forward  $f(\cdot)$  Learning under Domain Shift on Office dataset

Architectures		DSLRL	DSLRL	Amazon	Amazon	Webcam	Webcam
		↓ Amazon	↓ Webcam	↓ DSLRL	↓ Webcam	↓ DSLRL	↓ Amazon
ResNet-18	$f(\cdot)$	39.1	78	62.9	59	89.8	42.2
	$\mathcal{H}(\cdot)$	<b>47</b>	<b>90.7</b>	<b>67.3</b>	<b>63.9</b>	<b>96</b>	<b>44</b>
ResNet-34	$f(\cdot)$	41.8	83.3	<b>67.3</b>	60.1	90.6	41.7
	$\mathcal{H}(\cdot)$	<b>46.4</b>	<b>89.8</b>	<b>67.3</b>	<b>63.9</b>	<b>97.8</b>	<b>43.3</b>
ResNet-50	$f(\cdot)$	-	-	67.3	62	92.4	33.4
	$\mathcal{H}(\cdot)$	-	-	<b>78.1</b>	<b>68.4</b>	<b>97.8</b>	30.8
ResNet-101	$f(\cdot)$	-	-	62.9	59	89.8	31.77
	$\mathcal{H}(\cdot)$	-	-	<b>76.5</b>	<b>67.3</b>	<b>92.4</b>	<b>33.6</b>

back the 10,000 held-out images into the training set of  $f(\cdot)$  and the results match between Fig. 12a) and Fig. 12b).

Table 11: Performance of Proposed Introspective  $\mathcal{H}(\cdot)$  vs Feed-Forward  $f(\cdot)$  Learning under Domain Shift on VisDA Dataset

ResNet-18	Plane	Cycle	Bus	Car	Horse	Knife	Bike	Person	Plant	Skate	Train	Truck	All
$f(\cdot)$ (%)	27.6	7.2	<b>38.1</b>	54.8	43.3	<b>4.2</b>	<b>72.7</b>	<b>8.3</b>	28.7	22.5	<b>87.2</b>	2.9	38.1
$\mathcal{H}(\cdot)$ (%)	<b>39.9</b>	<b>27.6</b>	19.6	<b>79.9</b>	<b>73.5</b>	2.7	46.6	6.5	<b>43.8</b>	<b>30</b>	73.6	<b>4.3</b>	<b>43.58</b>

## C.6 Results on large images

### C.6.1 Domain Adaptation on Office dataset

In Section 4, we claim that introspection helps a network to better classify distributions that it has not seen while training. In Section 6, we tested on 95 new distributions in CIFAR-10C and 30 new distributions in CIFAR-10-CURE. In this section, we evaluate the efficacy of introspection when there is a domain shift between training and testing data under changes in background, and camera acquisition setup among others. Specifically, the robust recognition performance of  $\mathcal{H}(\cdot)$  is validated on Office [42] dataset using Top-1 accuracy. The Office dataset has 3 domains - images taken from either Webcam or DSLR, and extracted from Amazon website. Images can belong to any of 31 classes and they are of varying sizes - upto  $1920 \times 1080$ . Hence, results on Office shows the applicability of introspection on large resolution images. ImageNet pre-trained ResNet-18,34,50,101 [4] architectures are used for  $f(\cdot)$ . The final layer is retrained using the source domain while the remaining two domains are for testing. The experimental setup, the same detailed in Section 6, is applied and the Top-1 accuracy is calculated. The results are summarized in Table 10. In every instance, the top domain is  $\mathcal{X}$  - the training distribution, and the bottom domain is  $\mathcal{X}'$  - the testing distribution. Note that ResNet-50 and 101 failed to train on 498 images in DSLR source domain. The results of introspection exceed that of feed-forward learning in all but ResNet-50 when classifying between Webcam and Amazon domains.

### C.6.2 Domain Adaptation on Vis-DA dataset

Validation results on a synthetic-to-real domain shift dataset called VisDA [59] are presented in Table 11. VisDA has 12 classes with about 152,000 synthetic training images, and 55,000 real validation images. The validation images are cropped images from MS-COCO. ResNet-18 architecture pretrained on ImageNet is finetuned on the synthetically generated training images from VisDA dataset for 200 epochs. It is then tested on the validation images and the recognition performance is shown in Table 11 as feed-forward  $f(\cdot)$  results. Introspective  $\mathcal{H}(\cdot)$  results are obtained and shown when  $f(\cdot)$  is ResNet-18. There is an overall improvement of 5.48% in terms of performance accuracy. However, the individual class accuracies leave room for improvement.

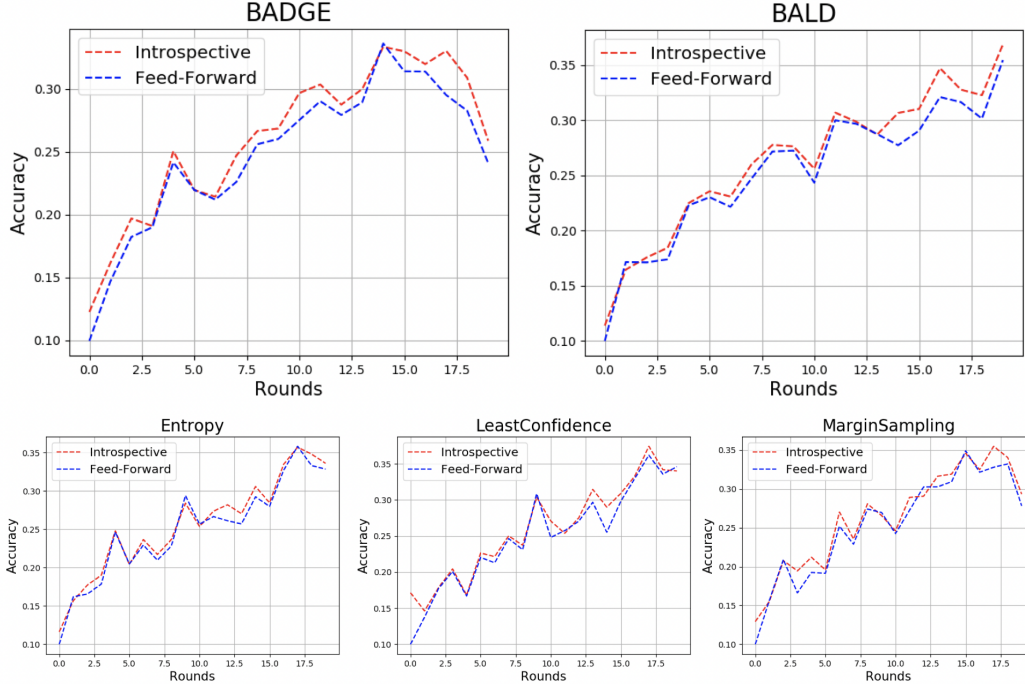


Figure 13: Introspective vs. Feed-Forward accuracy of ResNet-18 across training rounds for state-of-the-art techniques in an active learning setting. The query batch size per round is 1000. The trainset is CIFAR-10 and testset is Gaussian Noise from CIFAR-10C.

Table 12: Out-of-distribution Detection of existing techniques compared between feed-forward and introspective networks when the data is under adversarial attack.

Methods	OOD Datasets (Attack)	FPR (95% at TPR) ↓	Detection Error ↓	AUROC ↑
Feed-Forward/Introspective				
MSP [35]	Textures	99.98/ <b>23.19</b>	45.9/ <b>7.9</b>	30.4/ <b>96.48</b>
	iSUN	98.63/ <b>87.2</b>	46.71/ <b>28.95</b>	46.44/ <b>75.81</b>
	Places365	100/ <b>83.59</b>	47.64/ <b>26.46</b>	25.08/ <b>79</b>
	LSUN-C	99.65/ <b>87.64</b>	43.38/ <b>26.31</b>	43.47/ <b>78.4</b>
ODIN [36]	Textures	99.95/ <b>2.06</b>	47.7/ <b>3.48</b>	37.5/ <b>99.11</b>
	iSUN	96.8/ <b>90.42</b>	44.77/ <b>31.11</b>	53.88/ <b>73.22</b>
	Places-365	99.97/ <b>82.5</b>	47.12/ <b>26.86</b>	32.69/ <b>78.88</b>
	LSUN-C	98.6/ <b>88.28</b>	40.51/ <b>27.88</b>	56.7/ <b>77.25</b>

## D Appendix: Downstream Applications

### D.1 Active Learning

In Table 2, the mean recognition accuracies across the first 20 rounds of Active Learning experiments for commonly used query strategies are shown. We plot these recognition accuracies across for all five query strategies in Fig. 13. The x-axis is the round at which the performance is calculated. The calculated accuracy is plotted on the y-axis. The experiment starts with a random 100 images in round 1. Each strategy queries using either a round-wise sample trained  $f(\cdot)$  or a round-wise sample trained  $\mathcal{H}(\cdot)$ . Note that at each round, the networks are retrained. This continues for 20 rounds. Both BALD [34] and BADGE [33] applied on  $\mathcal{H}(\cdot)$  consistently beat its  $f(\cdot)$  counterpart on every round. This is because both these methods rely on extracting features from the network as compared to the other three techniques that directly use the output logits from either  $\mathcal{H}(\cdot)$  or  $f(\cdot)$ . Since the network is not well-trained at the initial stages - due to a dearth of training data - the introspective network is not as consistent as the feed-forward network among Entropy, Least Confidence, and Margin strategies. Nonetheless,  $\mathcal{H}(\cdot)$  outperforms  $f(\cdot)$  on average across all rounds.

Table 13: Performance of Contrastive Features against Feed-Forward Features and other Image Quality Estimators. Top 2 results in each row are highlighted.

Database	PSNR HA	IW SSIM	SR SIM	FSIMc	Per SIM	CSV	SUM MER	Feed-Forward UNIQUE	Introspective UNIQUE
<b>Outlier Ratio (OR, ↓)</b>									
MULTI	0.013	0.013	<b>0.000</b>	0.016	0.004	<b>0.000</b>	<b>0.000</b>	<b>0.000</b>	<b>0.000</b>
TID13	<b>0.615</b>	0.701	0.632	0.728	0.655	0.687	<b>0.620</b>	0.640	<b>0.620</b>
<b>Root Mean Square Error (RMSE, ↓)</b>									
MULTI	11.320	10.049	8.686	10.794	9.898	9.895	<b>8.212</b>	9.258	<b>7.943</b>
TID13	0.652	0.688	0.619	0.687	0.643	0.647	0.630	<b>0.615</b>	<b>0.596</b>
<b>Pearson Linear Correlation Coefficient (PLCC, ↑)</b>									
MULTI	0.801	0.847	0.888	0.821	0.852	0.852	<b>0.901</b>	0.872	<b>0.908</b>
	-1	-1	0	-1	-1	-1	-1	-1	
TID13	0.851	0.832	0.866	0.832	0.855	0.853	0.861	<b>0.869</b>	<b>0.877</b>
	-1	-1	0	-1	-1	-1	0	0	
<b>Spearman's Rank Correlation Coefficient (SRCC, ↑)</b>									
MULTI	0.715	<b>0.884</b>	0.867	0.867	0.818	0.849	<b>0.884</b>	0.867	<b>0.887</b>
	-1	0	0	0	-1	-1	0	0	
TID13	0.847	0.778	0.807	0.851	0.854	0.846	0.856	<b>0.860</b>	<b>0.865</b>
	-1	-1	-1	-1	0	-1	0	0	
<b>Kendall's Rank Correlation Coefficient (KRCC)</b>									
MULTI	0.532	<b>0.702</b>	0.678	0.677	0.624	0.655	0.698	0.679	<b>0.702</b>
	-1	0	0	0	-1	0	0	0	
TID13	0.666	0.598	0.641	0.667	<b>0.678</b>	0.654	0.667	0.667	<b>0.677</b>
	0	-1	-1	0	0	0	0	0	

## D.2 OOD

**Adversarial setting in Table 3** A datapoint  $z$ , is perturbed as  $z + \epsilon$  and the goal of the detector is to classify  $z \in \mathcal{X}$  or  $z \in \mathcal{X}'$ . This modality is proposed by the authors in [44] and we use their setup. PGD attack with perturbation 0.0014 is used. The same MSP and ODIN detectors from Table 3 are utilized. On 4 OOD datasets, both MSP and ODIN show a performance gain across all three metrics on  $\mathcal{H}(\cdot)$  compared to  $f(\cdot)$ . Note that the results in Table 12 is for ResNet-18 architecture for the same  $f(\cdot)$  and  $\mathcal{H}(\cdot)$  used in other experiments including Fig. 4.

**Vanilla setting in Table 12** In Table 12, we show the results of out-of-distribution detection when  $\mathcal{X}$  is CIFAR-10 and  $\mathcal{X}'$  are the four considered datasets. Note that among the four datasets, textures and SVHN are more out-of-distribution from CIFAR-10 than the natural image datasets of Places365 and LSUN. The results of the introspective network is highest on Textures DTD dataset.

## D.3 Image Quality Assessment

**Related Works** Multiple methods have been proposed to predict the subjective quality of images including PSNR-HA [60], IW-SSIM [61], SR-SIM [62], FSIMc [63], PERSIM [64], CSV [65], SUMMER [66], ULF [67], UNIQUE [39], and MS-UNIQUE [68]. All these methods extract structure related hand-crafted features from both reference and distorted images and compare them to predict the quality. Recently, machine learning models have been proposed to directly extract features from images [39]. [39] propose UNIQUE that uses a sparse autoencoder trained on ImageNet to extract features from both reference and distorted images. We use UNIQUE as our base network  $f(\cdot)$ .

**Feed-Forward UNIQUE** [39] train a sparse autoencoder with a one layer encoder and decoder and a sigmoid non-linearity on 100,000 patches of size  $8 \times 8 \times 3$  extracted from ImageNet testset. The autoencoder is trained with MSE reconstruction loss. This network is our  $f(\cdot)$ . UNIQUE follows a full reference IQA workflow which assumes access to both reference and distorted images while estimating quality. The reference and distorted images are converted to YGCr color space and converted to  $8 \times 8 \times 3$  patches. These patches are mean subtracted and ZCA whitened before being passed through the trained encoder. The activations of all reference patches in the latent space are extracted and concatenated. Activations lesser than a threshold of 0.025 are suppressed to 0. The choice of threshold 0.025 is made based on the sparsity coefficient used during training. Similar procedure is followed for distorted image patches. The suppressed and concatenated features of both the reference and distorted images are compared using Spearman correlation. The resultant is the feed-forward estimated quality of the distorted image.

**Introspective-UNIQUE** We use the architecture and the workflow from [39] which is based on feed-forward learning to demonstrate the value of introspection. We replace the feed-forward features with the proposed introspective features. The loss in Eq. 6 for introspection is not between classes but between the image  $x$  and its reconstruction  $\hat{x}$  from the sparse autoencoder from [39]. For a reference image  $x$ ,  $r_x$  is derived using  $J(x, \hat{x})$ . Hence, gradients of  $r_x$  span the space of reconstruction noise. Since the need in IQA is to characterize distortions, we obtain  $r_x$  for reference images from the first layer and project both reference and distorted images onto  $r_x$ . These projections are compared using Spearman correlation to assign a quality estimate. In this setting,  $\mathcal{H}(\cdot)$  is the projection operator and Spearman correlation. Hence, Introspective-UNIQUE broadens introspection in the following ways - 1) defining introspection on generative models, 2) using gradients in the earlier layers of a network.

**Statistical Significance** We use the statistical significance code and experimental modality from the Feed-Forward model [39]. Specifically, we follow the procedure presented for IQA statistical significance test regulations suggested by ITU-T Rec. P.1401. Normality tests are conducted on the human opinion scores within the datasets and those scores that significantly deviate from dataset-specific parameters are discarded. Hence, for the purpose of our statistical significance tests, we assume that the given scores are a good fit for normal distribution. The predicted correlation coefficients from the proposed Introspective-UNIQUE technique are compared individually against all other techniques in Table 13. For the test itself, we use Fisher-Z transformation to obtain the normally distributed statistic between the compared methods. A 0 corresponds to statistically similar performance between Introspective-UNIQUE and the compared method, -1 means that the compared method is statistically inferior to Introspective-UNIQUE, and 1 indicates that the compared method is statistically superior to Introspective-UNIQUE.

**Results** We report the results of the proposed introspective model in comparison with commonly cited methods Table 13. We utilize MULTI-LIVE (MULTI) [69] and TID2013 [70] datasets for evaluation. The performance is validated using outlier ratio (consistency), root mean square error (accuracy), Pearson correlation (linearity), Spearman correlation (rank), and Kendall correlation (rank). Arrows next to each metric in Table 13 indicate the desirability of a higher number ( $\uparrow$ ) or a lower number ( $\downarrow$ ). Two best performing methods for each metric are highlighted. The proposed framework is always in the top two methods for both datasets in all evaluation metrics. In particular, it achieves the best performance for all the categories except in OR and KRCC in TID2013 dataset. The feed-forward model does not achieve the best performance for any of the metrics in MULTI dataset. However, the same network using introspective features significantly improves the performance and achieves the best performance on all metrics. For instance, the feed-forward model is the third best performing method in MULTI dataset in terms of RMSE, PLCC, SRCC, and KRCC. However, the introspective features improve the performance for those metrics by 1.315, 0.036, 0.020, and 0.023, respectively and achieve the best performance for all metrics. This further reinforces the plug-in capability of the proposed introspective inference. Additionally, against no technique is our method not statistically significant in at least 1 metric.

#### D.4 Uncertainty

Table 14: Uncertainty quantification algorithms measured against Introspective Resnet-18. Accuracy is recognition accuracy.

Modality	Techniques	CIFAR-10-Rotations		
		Log-likelihood ( $\uparrow$ )	Brier Score ( $\downarrow$ )	Accuracy ( $\uparrow$ )
Ensemble	Bootstrap [71]	-2.03	0.71	0.47
Bayesian	MC Dropout [72]	-2.81	0.85	0.44
Bayesian	BBP without lrt [73]	-1.87	0.74	0.39
Bayesian	BBP with lrt [73]	-2.33	0.78	0.42
Deterministic	TENT [74]	-15.54	1.36	0.30
Deterministic	Introspective Resnet-18	-2.97	0.89	0.45

Existing methods of uncertainty quantification are compared against an Introspective Resnet-18 in Table. 14. Column 1 denotes the modality of the method. A deterministic method like the proposed introspection and TENT [74] require only a single pass through the network. Bayesian

networks require multiple passes. Ensemble techniques require multiple networks. We use two uncertainty measures, log-likelihood and brier score, to measure uncertainty. A detailed review of these measures is presented in [71]. For all methods, we use the same base Resnet-18 trained on the undistorted images from Section 6 as our architecture. A rotated version of CIFAR-10 testset is used to determine uncertainty. For every image there are 16 rotated versions of the same image. Hence, there are 160,000 images in the testset. The results are presented in Table 14. The ensemble method outperforms all other techniques both in terms of accuracy as well as uncertainty. However, the proposed introspective technique performs comparably to bayesian techniques among the uncertainty metrics while beating them in recognition accuracy. It outperforms TENT among both recognition accuracy and uncertainty metrics.

## E Appendix: Reproducibility Statement

The paper uses publicly available datasets to showcase the results. Our introspective learning framework is built on top of existing deep learning apparatus - including ResNet architectures [4] (inbuilt PyTorch architectures), CIFAR-10C data [27] (source code at <https://zenodo.org/record/2535967#.YLpTF-1KhhE>), calibration ECE and MCE metrics [37] (source code at [https://github.com/markus93/NN\\_calibration](https://github.com/markus93/NN_calibration)), out-of-distribution detection metrics, and codes for existing methods were adapted from [44] (source code at <https://github.com/jfc43/robust-ood-detection>), active learning methods and their codes were adapted from [33] (source code at <https://github.com/JordanAsh/badge>), Grad-CAM was adapted from [6] (code used is at [https://github.com/adityac94/Grad\\_CAM\\_plus\\_plus](https://github.com/adityac94/Grad_CAM_plus_plus)). Our own codes will be released upon acceptance. The exact training hyperparameters for  $f(\cdot)$  and  $\mathcal{H}(\cdot)$ , and all considered  $\mathcal{H}(\cdot)$  architectures are shown in Appendix C.1. Extensive ablation studies on  $\mathcal{H}(\cdot)$  are shown in C.4.